Vertebral Artery Occlusion in Duplex Color-Coded Ultrasonography

Kozue Saito, MD; Kazumi Kimura, MD; Kazuyuki Nagatsuka, MD; Keiko Nagano, MD; Kazuo Minematsu, MD; Satoshi Ueno, MD; Hiroaki Naritomi, MD

Background and Purpose—To establish the diagnostic criteria for the site of occlusion in the vertebral arteries (VAs) using duplex color-coded ultrasonography.

Methods—In 128 consecutive patients who underwent conventional cerebral angiography, we prospectively measured the diameter, mean flow velocity (MV), peak systolic flow velocity, and end-diastolic flow velocity of both VAs. The diameter-ratio (diameter of contralateral VA divided by that of target VA) and MV-ratio (MV of contralateral VA divided by that of target VA) were determined. Based on the angiographic findings, we classified the VAs into 4 types (5 groups) as follows: (1) the origin of VA occlusion (Origin group: n=9); (2) VA occlusion before branching into the posterior inferior cerebellar artery (PICA) (Before group: n=10); (3A) symptomatic VA occlusion after branching into the PICA (After group: n=12); (3B) asymptomatic or hypoplastic occlusive VA after branching into the PICA (PICA end group: n=15); and (4) no significant occlusive lesions in the VA (Control group: n=194).

Results—No flow signals in the VAs apparently indicated the Origin group. Preserved peak systolic flow velocity but end-diastolic flow velocity of zero cm/s indicated the Before group. MV <18 cm/s and MV-ratio ≥1.4 indicated the PICA end group or After group. Furthermore, these groups could be distinguished as follows: a diameter-ratio <1.4 indicated the After group. A diameter-ratio ≥1.4 indicated the PICA end group. Either MV ≥18 cm/s or MV <18 cm/s in combination with MV-ratio <1.4 indicated the Control group.

Conclusion—Duplex color-coded ultrasonography can accurately diagnose the site of VA occlusion. (***Stroke*. 2004;35: 1068-1072.)**

Key Words: vertebral artery ■ occlusion ■ ultrasonography ■ ultrasonography, Doppler, duplex ■ diagnosis ■ vertebrobasilar circulation

Duplex color-coded ultrasonography is useful in the evaluation of occlusive lesions in the carotid[1–6] and vertebral[7–13] arteries (VAs) in acute stroke patients. The diagnostic criteria for occlusive lesions in the carotid arteries have been already established.[1,5] Duplex color-coded ultrasonography is also valuable to evaluate pathological VAs, such as VA occlusion,[13,14] subclavian steal phenomenon,[12,15–17] and vertebral arterial dissection.[18–21] The site of VA occlusions is divided into 3 groups: VA origin occlusions, VA occlusions before branching into the posterior inferior cerebellar artery (PICA), and VA occlusions after branching into the PICA. However, the diagnostic criteria in duplex ultrasonography for the site of VA occlusion remain unclear. Furthermore, a few VAs show asymptomatic occlusion or naturally hypoplastic VA ending at the PICA (PICA end).[22] The aim of the present study was to establish the criteria for determining the site of occlusion of VAs, including VAs ending at the PICA, using duplex color-coded ultrasonography.

Methods

We prospectively assessed the 256 VAs of 128 consecutive patients (91 men and 37 women, mean±SD; 63.4±12.2 years) admitted to the National Cardiovascular Center and who underwent intraarterial digital subtraction angiography (IA-DSA) between May 1, 2003 and July 31, 2003. We excluded 16 VAs with 50% to 99% stenosis in diameter on angiography because the flow velocity was also affected by the stenotic lesions. Therefore, 240 VAs were examined in the present study. Eighty-four patients had acute cerebral infarctions (33 in the vertebrobasilar circulation and 51 in the internal carotid arterial circulation), 12 had transient ischemic attacks, 20 had old infarctions (12 in the vertebrobasilar circulation, 8 in the internal carotid arterial circulation), 3 had cerebral hemorrhages, and the remaining 9 nonstroke patients had asymptomatic arterial stenotic or occlusive lesions (1 in the basilar artery, 2 in the middle cerebral artery, and 6 in the internal carotid artery). Eighty-four patients with acute stroke underwent IA-DSA within 2.6±3.9 days of stroke onset. Informed consent for IA-DSA was obtained from both the patient and family.

Selective IA-DSA was performed using a biplane, high-resolution angiography system (Angio Rex Super-G and DFP-2000A; Toshiba) with a matrix of 1024×1024 pixels. A catheter was inserted into the right brachial artery or femoral artery in accordance with the

Received December 27, 2003; accepted January 30, 2004.

From Cerebrovascular Division (K.S., K.K., K.Nagatsuka, K.Nagano, K.M., H.N.), Department of Medicine, National Cardiovascular Center, Japan; Department of Neurology (S.U.), Nara Medical University, Japan.

Correspondence to Dr Kozue Saito, Fujishirodai, Suita, Osaka 565-8565, Japan. E-mail ksaito@hsp.ncvc.go.jp

Stroke is available at http://www.strokeaha.org

DOI: 10.1161/01.STR.0000125857.63427.59

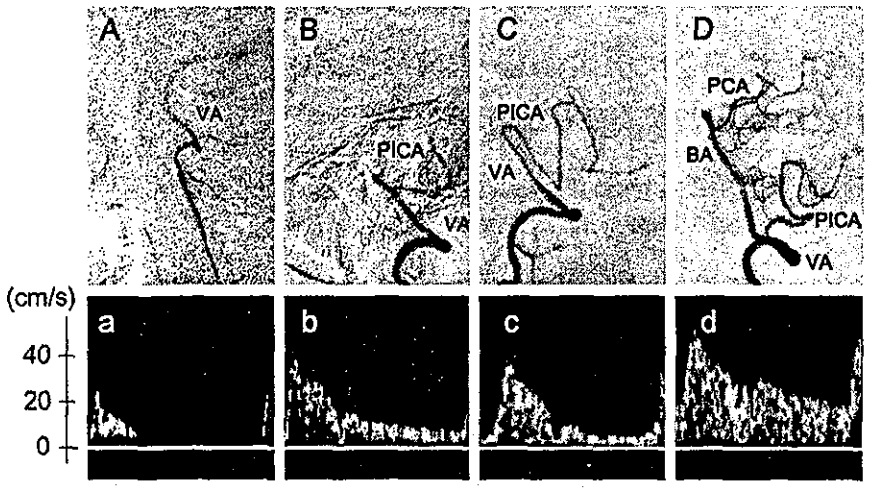

Figure 1. Angiogram (lateral view of vertebral arterial angiography) and Doppler waveforms of patients in the Before group (A and a), After group (B and b), PICA end group (C and c), and Control group (D and d). A and a, The VA was occluded before branching into the PICA. The Doppler waveform showed no EDV. B and b, The VA was occluded after branching into the PICA. The Doppler waveform showed EDV and MV was lower than those of the Control group. C and c, The VA ended in the PICA and did not continue to the union of the BA. The Doppler waveform also showed EDV and MV were lower than those of the Control group. D and d, No significant occlusion of the VA. The Doppler waveform showed EDV and MV was highest among all groups. VA indicates vertebral artery; BA, basilar artery; PICA, posterior inferior cerebellar artery; PCA, posterior cerebral artery.

Seldinger method, and then guided to the cerebral arteries for diagnostic 4-vessel angiography. Based on the angiographic findings, we classified the VA vessels into 4 types (5 groups) as follows: (1) the origin of VA occlusion (Origin group); (2) VA occlusion before branching into the PICA (Before group); (3) VA occlusion after branching into the PICA, which was divided into 2 groups—(3A) VA symptomatic occlusion after branching into the PICA (After group) and (3B) hypoplastic or asymptomatic occlusive VA after branching into the PICA (PICA end group); and (4) no significant occlusive lesions in the VAs (Control group). The After group was defined as symptomatic VA occlusion associated with acute ischemic stroke presented as a new infarct on MRI including diffusion-weighted imaging (DWI) or transient ischemic attack (TIA) in the vertebrobasilar circulation. The clinical diagnosis of stroke and TIA was made by the attendant physician from the result of MRI (DWI) and neurological findings. When VA occlusion was symptomatic, we identified it as the After group, even if the diameter of the target VA was smaller than that of the contralateral VA.

Using B-mode scans with color imaging and pulsed-Doppler, one investigator with no previous knowledge of the patients' clinical information including angiographic findings (K.S.) measured the flow velocities of both VAs within 48 hours before or after IA-DSA. We used a Sonos 5500 duplex color-coded ultrasonographic device (Philips) equipped with a 7.5-MHz transducer. First, we measured the diameter of the both VAs at the C3–4, C4–5, or C5–6 levels. Second, the flow velocities of the VAs were obtained between the transverse process at the C3–4, C4–5, or C5–6 levels of the cervical spine. The sample volume (2 to 3 mm, depending on the diameter of the VA) was set within the VAs and flow velocities were measured, taking care to maintain an adequate angle of ≤60 degrees between the beam and the VAs. The pulse repetition frequency was 3.0 or 3.5 Hz, and the low pass filter was set at 70 Hz. We obtained the peak systolic flow velocity (PSV), the end-diastolic flow velocity (EDV), and the time-averaged peak mean flow velocity (MV), corrected using the adequate angle for both VAs. Resistance index (RI) was defined as (PSV-EDV)÷PSV. The diameter-ratio (diameter of contralateral VA divided by diameter of target VA) and MV-ratio (MV of contralateral VA divided by that of target VA) were also determined. The diameter, diameter-ratio, and flow velocity data for each group were expressed as mean±SD.

Brain computed tomography (CT) and MRI including DWI were performed in all the patients to assess new brain infarctions. Conventional MRI T1-weighted (repetition time [TR]/echo time [TE]; 630/14), T2-weighted (TR/TE; 5400/99), and fluid-attenuation inversion recovery (FLAIR) (TR/TE; 9000/105) images were obtained. DWI was performed simultaneously using a spin-echo planar imaging sequence. Diffusion gradients were applied in the x, y, and z directions, with a b value of 1000/cm^2.

Statistical analysis was performed using the Mann-Whitney U test and Kruskal-Wallis test. A value of $P<0.05$ was accepted as indicating statistical significance. Sensitivity and specificity curves were produced to obtain the best cut-off value for each diagnostic criterion.

Results

The VAs were clearly displayed in all patients using B-mode with color imaging, and blood flow velocity was successfully evaluated by pulse Doppler (Figure 1). Table 1 shows the VA diameter, diameter-ratio, MV, MV-ratio, EDV, and RI of each VA.

Origin Group

Although the VAs were clearly detected using B-mode with color imaging, no blood flow signals, including MV and

TABLE 1. Parameters in Each Group

Group	N of Vessels	VA Diameter (mm)	Diameter-ratio	MV (cm/s)	MV-ratio	EDV (cm/s)	RI
Control	194	3.76±0.66	0.97±0.27	25.26±7.54	0.94±0.37	15.10±5.39	0.66±0.09
Origin	9	3.25±1.08	1.39±0.31	0	—	0	—
Before	10	3.25±0.72	1.20±0.42	7.24±4.64	2.38±1.55	0	1
After	12	3.37±0.64	1.10±0.23	12.92±3.29	2.00±0.80	6.69±3.74	0.78±0.14
PICA end	15	2.62±0.39	1.68±0.31	13.95±3.22	2.31±1.73	7.09±2.46	0.76±0.09
Total	240						

Diameter-ratio indicates diameter of contralateral VA divided by that of target VA; MV, mean flow velocity; MV-ratio, mean flow velocity of contralateral VA divided by that of target VA; EDV, end-diastolic flow velocity; RI, resistance index=(peak systolic flow velocity−end-diastolic flow velocity)÷peak systolic flow velocity.

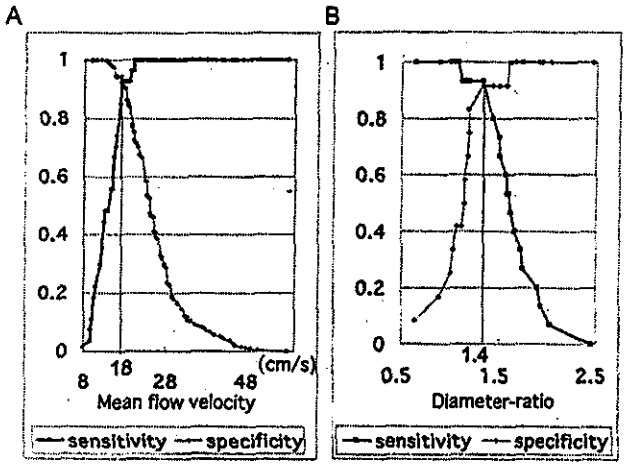

Figure 2. A, Sensitivity and specificity curve analysis for MV to discriminate the After and PICA-end groups from the Control group. B, Sensitivity and specificity curve analysis for diameter-ratio to discriminate the PICA end group from the After group.

EDV, in the VAs could be detected using pulse Doppler, allowing the Origin group VAs to be easily identified.

Before Group

Peak systolic flow velocity was preserved, but EDV was zero cm/s in all patients in the Before group. In addition, the MV (7.2±4.6 cm/s) was the lowest among all the groups, excluding the Origin group ($P<0.0001$). Excluding the Origin group, an EDV of zero cm/s allowed the Before group VAs to be easily distinguished from the other groups.

Distinguishing After and PICA End Groups From the Control Group

Of the 3 groups other than the Origin and Before groups, the MV, EDV, and RI of the After and PICA end groups (After group:12.9±3.3 cm/s, 6.7±3.7 cm/s, 0.78±0.14, respectively; PICA end group:14.0±3.2 cm/s, 7.1±2.5 cm/s, 0.76±0.09, respectively) were lower than those of the Control group (25.3±7.5 cm/s, 15.1±5.4 cm/s, 0.66±0.09, respectively) ($P<0.0001$). Using sensitivity–specificity curve analysis for discriminating the Control group from the After and PICA end group, the cut-off point of the RI and MV were 0.7 (sensitivity 74.0% and specificity 72.6%) and 18 cm/s (sensitivity 92.6% and specificity 90.2%; Figure 2A), respectively. Therefore, MV was a better parameter than RI for discriminating the After and PICA end groups from the Control group. However, 18 of 43 patients with MV <18 cm/s belonged to the Control group and the positive predictive value was low (58.1%). Of these 43 VAs with MV <18 cm/s, the sensitivity–specificity curve for MV-ratio to distinguish the After and PICA end groups from the Control group showed a cut-off value of 1.4 and gave a sensitivity of 84.0% and specificity of 82.3%. If we used the combined criteria of both MV <18 cm/s and MV-ratio ≥1.4 to distinguish the After and PICA end groups from the Control group, then sensitivity, specificity, accuracy, and positive predictive value were 85.2%, 97.4%, 95.9%, and 82.1%, respectively.

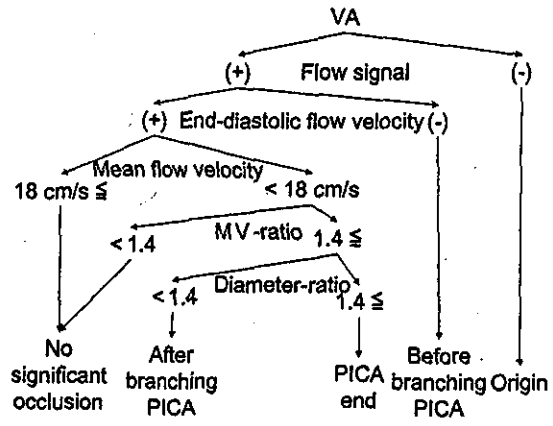

Figure 3. Ultrasonographic diagnostic algorithm for the site of VA occlusion.

Distinguishing the PICA End Group From the After Group

No significant difference in MV, EDV, and RI between the After group and PICA end group was observed. However, the diameter (2.62±0.39 mm) in the PICA end group was the smallest among all the groups (Before group: 3.25±0.72 mm; After group: 3.37±0.64 mm; Control group: 3.76±0.66 mm) ($P<0.0001$). The diameter-ratio (1.68±0.31) in the PICA end group was also the largest among all the groups (Before group: 1.20±0.42; After group: 1.10±0.23; Control group: 0.97±0.27, respectively) ($P<0.0001$). Using sensitivity–specificity curve analysis for discriminating the PICA end group from the After group, the cut-off point of VA diameter and diameter-ratio were 2.8 mm (sensitivity 73.3% and specificity 83.3%) and 1.4 (sensitivity 93.3% and specificity 91.7%), respectively (Figure 2B). Therefore, the diameter-ratio was a better parameter than VA diameter for discriminating the PICA end group from the After group.

Ultrasonographic Diagnostic Criteria

Figure 3 shows the criteria for the site of VA occlusion, including PICA end with duplex color-coded ultrasonography based on the present results. Table 2 shows the relationship between the cerebral angiographic findings and our ultrasonographic diagnosis. One VA vessel of the After group had the diameter-ratio ≥1.4. Therefore, we classified it as the PICA end, based on ultrasonographic criteria. The accuracy for conformity between them was 95.0%.

Discussion

The present study has established the ultrasonographic diagnostic criteria for determining the site of VA occlusion. Kimura et al[14] demonstrated the usefulness of measurement of VA flow velocity using duplex ultrasonography for the localization of the site of VA occlusion. They reported EDV of zero cm/s in a VA occlusion sited before branching into the PICA, which is consistent with the present findings. Furthermore, they described that the MV was significantly lower in a VA occlusion after branching into the PICA than in the nonocclusive VA group. However, accurate diagnostic criteria for differentiating these types were not established in their study.

TABLE 2. Comparison of Angiographic and Ultrasonographic Diagnoses

		Ultrasonographic Diagnosis					
		Control	Origin	Before	After	PICA End	Total
Angiographic Diagnosis	Control	189	0	0	3	2	194
	Origin	0	9	0	0	0	9
	Before	0	0	10	0	0	10
	After	2	0	0	9	1	12
	PICA end	2	0	1	1	11	15
	Total	193	9	11	13	14	240

In the present study, except for patients in the Origin and Before groups, 98.9% of patients with MV ≥18 cm/s had nonocclusive VAs, whereas 41.9% of patients with MV <18 cm/s also had nonocclusive VAs. Therefore, the criteria of threshold of MV <18 cm/s alone were insufficient to accurately distinguish the After group from the Control group. Using the combination of both MV-ratio ≥1.4 and MV <18 cm/s, sensitivity, specificity, accuracy, and positive predictive value to distinguish the After and PICA end groups from the Control group were much better at 85.2%, 97.4%, 95.9%, and 82.1%, respectively.

The VA blood flow wave and velocity between the After and PICA end groups were similar. Thus, we were unable to distinguish these groups by blood flow alone. Most hypoplastic VAs end in the PICA, and hypoplastic VA has been defined as a VA diameter of <2 mm.[13,23–25] In the present study, the mean and range of VA diameter in the PICA end group were certainly small, at 2.62±0.39 mm and 1.70 to 3.14 mm, respectively, and the PICA end group diameter was the smallest among the 5 groups. Therefore, the hypoplastic VA criteria of <2 mm may be high in specificity but low in sensitivity. When we used a cut-off value of 2.8 mm obtained from sensitivity and specificity curve analysis to distinguish the PICA end group from the After group, the accuracy was 77.8%, which was not overly useful. However, when we used a diameter-ratio ≥1.4 for the analysis, the sensitivity, specificity, and accuracy increased to 93.3%, 91.7%, and 92.6%, respectively, which was superior to that obtained using a cut-off VA diameter value of 2.8 mm. Therefore, a diameter-ratio ≥1.4 was identified as the criterion with which to differentiate between the After and PICA end groups. Diameter-ratio of symptomatic VAs occlusion was usually <1.4. In this study, however, we had 1 symptomatic VA occlusion with the diameter-ratio ≥1.4, which was diagnosed as PICA end by ultrasonography. This point may be one of the limitations in the present study.

Nicolau et al[13] examined RI in VA occlusion but did not discriminate the site of VA occlusion between before and after branching into the PICA. They reported that the RI in VA occlusion was higher than in non-VA occlusion. In the present study, although RI was higher in the After group than in the other groups, MV was superior to RI as a parameter to determine VA occlusion.

In the present study, the MV in 15 (18 vessels) of 117 patients in the Control group was <18 cm/s. Of these 15, 3 had an occlusion at the top of the basilar artery (BA), and 3 had bilateral fetal type of the posterior cerebral arteries (PCA). The blood flow of the VAs may be decreased under such conditions. This finding represents a limitation to the use of our criteria for identification of VA occlusion site.

We did not have any stenotic VAs in our present study. When the origin of VAs had stenosis, the blood flow velocity sometime reduces. Bray et al[26] reported that the velocity curve of severe stenotic VAs with their origin showed isolated ascending and lengthened systolic time and a systolic notch. Therefore, we should be able to distinguish it from the distal VA occlusion.

Another limitation is that asymptomatic acquired VA occlusion cannot always be distinguished from naturally hypoplastic VA ending in the PICA, as differentiating them is difficult in some patients, even with the findings of IA-DSA, MRI, and clinical symptoms. Therefore, the PICA end group may include asymptomatic acquired VA occlusion. In addition, in the present study, there were no patients with bilateral VA occlusion after branching into the PICA. Such patients may have been erroneously assigned into the Control group, because the MV-ratio in patients with bilateral VA occlusion would have been <1.4. Therefore, if a patient's neurological findings suggest occlusive lesions of the BA or VA after branching into the PICA, and the MV of both VAs is <18 cm/s and the MV-ratio is <1.4, those vessels would need to be assessed by transcranial Doppler or transcranial color-coded sonography.

In conclusion, measurement of the blood flow velocity and diameter of the VAs using duplex color-coded ultrasonography can help diagnose the site of VA occlusion. Ultrasonography is a noninvasive tool and can be performed bedside immediately after stroke patient admission. The present VA occlusion criteria may be used to evaluate VA occlusive lesions in acute stroke patients, in particular, those with medullary and brain stem infarction.

References

1. Moneta GL, Edwards JM, Chitwood RW, Taylor LM Jr, Lee RW, Cummings CA, Porter JM. Correlation of North Am Symptomatic Carotid Endarterectomy Trial (NASCET) angiographic definition of 70% to 99% internal carotid artery stenosis with duplex scanning. *J Vasc Surg.* 1993;17:152–159.
2. Kimura K, Yasaka M, Minematsu K, Wada K, Uchino M, Yonemura K, Ogata J, Yamaguchi T. Oscillating thromboemboli within the extracranial internal carotid artery demonstrated by ultrasonography in patients with acute cardioembolic stroke. *Ultrasound Med Biol.* 1998;24:1121–1124.
3. Kimura K, Yonemura K, Terasaki T, Hashimoto Y, Uchino M. Duplex carotid sonography in distinguishing acute unilateral atherothrombotic from cardioembolic carotid artery occlusion. *AJNR Am J Neuroradiol.* 1997;18:1447–1452.

4. Wada K, Kimura K, Minematsu K, Yasaka M, Uchino M, Yamaguchi T. Combined carotid and transcranial color-coded sonography in acute ischemic stroke. *Eur J Ultrasound.* 2002;15:101–108.
5. Yasaka M, Omae T, Tsuchiya T, Yamaguchi T. Ultrasonic evaluation of the site of carotid axis occlusion in patients with acute cardioembolic stroke. *Stroke.* 1992;23:420–422.
6. Wolverson MK, Heiberg E, Sundaram M, Tantanasirviongse S, Shields JB. Carotid atherosclerosis: high-resolution real-time sonography correlated with angiography. *AJR Am J Roentgenol.* 1983;140:355–361.
7. Trattnig S, Hubsch P, Schuster H, Polzleitner D. Color-coded Doppler imaging of normal vertebral arteries. *Stroke.* 1990;21:1222–1225.
8. Trattnig S, Schwaighofer B, Hubsch P, Schwarz M, Kainberger F. Color-coded Doppler sonography of vertebral arteries. *J Ultrasound Med.* 1991;10:221–226.
9. Bendick PJ, Jackson VP. Evaluation of the vertebral arteries with duplex sonography. *J Vasc Surg.* 1986;3:523–530.
10. Bartels E, Fuchs HH, Flugel KA. Duplex ultrasonography of vertebral arteries: examination, technique, normal values, and clinical applications. *Angiology.* 1992;43:169–180.
11. Davis PC, Nilsen B, Braun IF, Hoffman JC Jr. A prospective comparison of duplex sonography vs angiography of the vertebral arteries. *AJNR Am J Neuroradiol.* 1986;7:1059–1064.
12. Kimura K, Yamaguchi T, Yasaka M, Tsuchiya T. [Hemodynamics of the vertebral artery in subclavian steal syndrome and subclavian steal phenomenon]. *Rinsho Shinkeigaku.* 1991;31:970–973.
13. Nicolau C, Gilabert R, Chamorro A, Vazquez F, Bargallo N, Bru C. Doppler sonography of the intertransverse segment of the vertebral artery. *J Ultrasound Med.* 2000;19:47–53.
14. Kimura K, Yasaka M, Moriyasu H, Tsuchiya T, Yamaguchi T. Ultrasonographic evaluation of vertebral artery to detect vertebrobasilar axis occlusion. *Stroke.* 1994;25:1006–1009.
15. Hennerici M, Klemm C, Rautenberg W. The subclavian steal phenomenon: a common vascular disorder with rare neurologic deficits. *Neurology.* 1988;38:669–673.
16. Yip PK, Liu HM, Hwang BS, Chen RC. Subclavian steal phenomenon: a correlation between duplex sonographic and angiographic findings. *Neuroradiology.* 1992;34:279–282.
17. Kliewer MA, Hertzberg BS, Kim DH, Bowie JD, Courneya DL, Carroll BA. Vertebral artery Doppler waveform changes indicating subclavian steal physiology. *AJR Am J Roentgenol.* 2000;174:815–819.
18. Touboul PJ, Mas JL, Bousser MG, Laplane D. Duplex scanning in extracranial vertebral artery dissection. *Stroke.* 1988;19:116–121.
19. Bartels E, Flugel KA. Evaluation of extracranial vertebral artery dissection with duplex color-flow imaging. *Stroke.* 1996;27:290–295.
20. Hoffmann M, Sacco RL, Chan S, Mohr JP. Noninvasive detection of vertebral artery dissection. *Stroke.* 1993;24:815–819.
21. Sturzenegger M, Mattle HP, Rivoir A, Rihs F, Schmid C. Ultrasound findings in spontaneous extracranial vertebral artery dissection. *Stroke.* 1993;24:1910–1921.
22. Osborn AG. The vertebrobasilar system. In: Osborn AG, ed. *Cerebral angiography.* 2nd ed. Philadelphia: Lippincott Williams &Wilkins; 1999: 173–194.
23. Delcker A, Diener HC. [Various ultrasound methods for studying the vertebral artery—a comparative evaluation]. *Ultraschall Med.* 1992;13: 213–220.
24. Tegeler CH, Babikian VL, Gomez CR. Vertebral sonography. *Neurosonology.* 1996;91–92.
25. Fisher CM, Gore I, Okabe N, White PD. Atherosclerosis of the carotid and vertebral arteries—extracranial and intracranial. *J Neuropathol Exp Neurol.* 1965;24:455–476.
26. de Bray JM, Pasco A, Tranquart F, Papon X, Alecu C, Giraudeau B, Dubas F, Emile J. Accuracy of color-Doppler in the quantification of proximal vertebral artery stenoses. *Cerebrovasc Dis.* 2001;11:335–340.

Research article Related Commentary, page 312

Administration of CD34+ cells after stroke enhances neurogenesis via angiogenesis in a mouse model

Akihiko Taguchi,[1] Toshihiro Soma,[2] Hidekazu Tanaka,[3] Takayoshi Kanda,[4] Hiroyuki Nishimura,[5] Hiroo Yoshikawa,[5] Yoshitane Tsukamoto,[6] Hiroyuki Iso,[7] Yoshihiro Fujimori,[8] David M. Stern,[9] Hiroaki Naritomi,[1] and Tomohiro Matsuyama[5]

[1]Department of Cerebrovascular Disease, National Cardiovascular Center, Osaka, Japan. [2]Department of Hematology, Osaka Minami National Hospital, Osaka, Japan. [3]Department of Pharmacology, Graduate School of Medicine, Osaka University, Osaka, Japan. [4]Department of Gynecology, Osaka Minami National Hospital, Osaka, Japan. [5]Department of Internal Medicine, Hyogo College of Medicine, Hyogo, Japan. [6]Department of Pathology, Osaka Medical Center for Cancer and Cardiovascular Disease, Osaka, Japan. [7]Department of Psychology and [8]Department of Hematology, Hyogo College of Medicine, Hyogo, Japan. [9]Medical College of Georgia, Augusta, Georgia, USA.

Thrombo-occlusive cerebrovascular disease resulting in stroke and permanent neuronal loss is an important cause of morbidity and mortality. Because of the unique properties of cerebral vasculature and the limited reparative capability of neuronal tissue, it has been difficult to devise effective neuroprotective therapies in cerebral ischemia. Our results demonstrate that systemic administration of human cord blood–derived CD34+ cells to immunocompromised mice subjected to stroke 48 hours earlier induces neovascularization in the ischemic zone and provides a favorable environment for neuronal regeneration. Endogenous neurogenesis, suppressed by an antiangiogenic agent, is accelerated as a result of enhanced migration of neuronal progenitor cells to the damaged area, followed by their maturation and functional recovery. Our data suggest an essential role for CD34+ cells in promoting directly or indirectly an environment conducive to neovascularization of ischemic brain so that neuronal regeneration can proceed.

Introduction

Thrombo-occlusive atherosclerotic cardiovascular disease is a major cause of death and disability in developed countries. In the acute phase, therapeutic maneuvers include fibrinolytic therapy to restore blood flow to the ischemic site. In the longer term, formation of new blood vessels is necessary to fully supply tissue metabolic and functional requirements. Although it had been assumed that postnatal development of neovessels resulted only from outgrowth of pre-existing vasculature, it has become evident that circulating endothelial progenitor cells (EPCs), contained in a CD34+ cell population enriched in cord blood, have the capacity to participate in neovascularization of ischemic tissues (1, 2). Thus, a new strategy proposed for enhancing recovery due to ischemic stress is administration of EPCs to stimulate formation of neovasculature. In this context, recent reports have demonstrated that infusion of EPCs results in their incorporation into neovasculature at the ischemic site and limitation of tissue damage in animal models (3). Furthermore, human CD34+ cells were shown to secrete numerous angiogenic factors, including VEGF, HGF, and IGF-1 (4). On the basis of these observations, clinical trials of cell transplantation in hindlimb (5, 6) and cardiac ischemia (7) have been initiated with promising results.

Stroke is another setting of occlusive thromboatherosclerotic disease in which acceleration of angiogenesis might be expected to enhance the outcome. Despite the improvement of poststroke neurological outcome by administration of human cord blood cells (8) or bone marrow–derived cells (9) (both potentially a rich sources of stem cells including CD34+ cells) in rodent models, few of the administered cells could be demonstrated in brain parenchyma expressing neuronal markers, raising a question as to the underlying mechanism. The results of our study demonstrate that systemic administration of human CD34+ cells to immunocompromised mice subjected to stroke 48 hours earlier accelerates neovascularization of the ischemic zone. Such a rich vascular environment, along with generation of other nurturing neuronal mediators by CD34+ cells, such as VEGF, FGF2, and IGF-1 (10–12), enhances subsequent neuronal regeneration; endogenous neurogenesis is accelerated as neuronal progenitors migrate to the damaged area, followed by their maturation and survival when CD34+ cells have stimulated the formation of increased vascular channels. In contrast, in the presence of an antiangiogenic agent, the beneficial effect of CD34+ cells was lost. Our results provide the first direct link between vasculogenesis and neurogenesis in the repair of ischemic brain lesions.

Results

Induction of stroke and proliferation of endothelial cells in situ. A reproducible model of stroke in the middle cerebral artery (MCA) cortex, sparing the striatum, was developed in SCID mice by permanent ligation of the M1 distal portion of the left MCA. Subsequent infusion of carbon black showed strongly decreased staining in the affected area. Nonviability of affected tissue was confirmed by 2,3,5-triphenyltetrazolium (TTC) staining. Values of cortical width index (see Methods section) were highly reproducible (~0.34–0.36)

Nonstandard abbreviations used: anterior cerebral artery (ACA); cerebral blood flow (CBF); chloromethylbenzamido (CM-DiI); doublecortin (DCX); endothelial progenitor cell (EPC); erythropoietin (EPO); fetal liver kinase-1 (Flk-1); high-power field (HPF); middle cerebral artery (MCA); neuronal progenitor cell (NPC); neuron-specific nuclear protein (NeuN); phycoerythrin (PE); polysialylated neuronal cell adhesion molecule (PSA-NCAM); subventricular zone (SVZ); 2,3,5-triphenyltetrazolium (TTC).

Conflict of interest: The authors have declared that no conflict of interest exists.

Citation for this article: *J. Clin. Invest.* 114:330–338 (2004). doi:10.1172/JCI200420622.

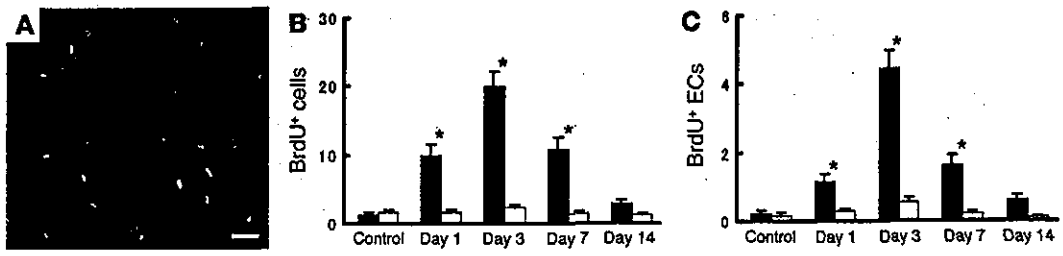

Figure 1
Endothelial proliferation in situ after stroke. On days 1, 3, 7, and 14 after stroke, the number of proliferating cells (BrdU+) and proliferating endothelial cells (co-staining for BrdU and CD31) was determined in the left cortical area of 1–1.5 mm distal from the midline. (**A**) Immunohistological analysis of proliferating cells labeled with BrdU (green), anti-mouse CD31 IgG (red), and both (yellow). The number of cells visualized with BrdU (**B**) and the subpopulation BrdU+ cells also displaying mouse CD31 (i.e., double positives) (**C**) are shown. Ten HPFs were evaluated for each animal ($n = 6$ per group) by two investigators blinded to the experimental protocol. Note in **C**, cells displaying mouse CD31 are termed endothelial cells (ECs). Black bars, ipsilateral; white bars, contralateral. *$P < 0.05$ versus control. Scale bar: 30 μm.

over the 12-week experimental period. Survival in this stroke model was greater than 95%, and no seizures were observed.

To estimate the optimal time to administer human CD34+ cells, proliferation of endothelial cells in vasculature of the penumbral region (at the leading edge of viable tissue) was assessed by in vivo BrdU labeling. Sections were visualized with antibody to BrdU and mouse-specific antibody to CD31 by confocal microscopy. Cellular profiles co-staining for both markers were considered proliferating endothelial cells (Figure 1A). On days 1 and 3 after stroke, a subpopulation of BrdU+ cells also stained with mouse CD31, indicating an endothelial origin of this signal (Figure 1, B and C). By day 7, although endothelial proliferation continued, it had begun to decrease. In contrast, BrdU-labeled cells were present in a constant, small amount on the contralateral (nonstroke) side (Figure 1, B and C). These data indicated that administration of CD34+ cells on day 2 after stroke would buttress the endogenous proliferative component of the vascular response to cerebral ischemia.

Administration of CD34+ cells after stroke. Human CD34+ cells (95% pure CD34+ cells) isolated from human cord blood or control cells (CD34- cells with <0.2% CD34+ cells, also from human cord blood) were administered intravenously via tail vein 48 hours after stroke. Analysis of cell surface markers revealed that 1.5% ± 0.1% and 0.9% ± 0.1% of the CD34+ cell population expressed the endothelial lineage markers fetal liver kinase-1 (Flk-1) (1) and P1H12 (13), respectively ($n = 4$). The effect of CD34+ cells was evident within 24 hours of their transplantation. Labeling vasculature by infusion of carbon black ink demonstrated neovasculature at the border of the MCA and anterior cerebral artery (ACA) cortex (staining with TTC demarcates viable and nonviable tissue) in animals treated with CD34+ cells (Figure 2, A and B), compared with those receiving CD34- cells (Figure 2C) or PBS alone (Figure 2D). Determination of the angiographic score confirmed the impression of increased neovasculature in animals transplanted with CD34+ cells, compared with other groups (Figure 2E). To evaluate vascular activation in affected cerebral vessels, we used mouse-specific antibody to CD13, an antigen expressed by endothelial cells in angiogenic, but not quiescent, vasculature (14). Visualization of mouse CD13 in brain sections 24 hours after cell transplantation showed that cells bearing this activated endothelial marker were most evident in sections from mice treated with CD34+ (Figure 2F), compared with those receiving CD34- cells (Figure 2G) or PBS (Figure 2H). Increased density of vasculature in the ischemic territory of animals treated with CD34+ cells translated to significantly enhanced cerebral blood flow (CBF) (Figure 2I).

To analyze the effect of subpopulations within the general CD34+ cell population, we compared the effect of poststroke transplantation of the same number of CD34+ cells (containing Flk-1- and Flk-1+ cells) with CD34+/Flk-1- cells on vascular activation and neovascularization. Brain tissue was examined 7 days after cell transplantation, because EPCs are known to incorporate into capillary walls at ischemic sites by this time point after the ischemic episode (2). FACS analysis confirmed that the CD34+/Flk-1- population contained less than 0.1% Flk-1+ cells ($n = 4$). On the basis of CD13 staining (using the same mouse-specific antibody mentioned earlier), there was similar activation of endogenous endothelium after transplantation of either CD34+ cells (including both Flk-1- and Flk-1+ subpopulations) and CD34+/Flk-1- cells (not shown). Although neovasculature was observed at the border of the MCA and ACA cortex in animals treated with CD34+ cells (Figure 2J) and CD34+/Flk-1- cells (Figure 2K), mice treated with CD34+ cells displayed increased neovascularization based on angiographic score (scores of 22 ± 3 and 13 ± 2, for CD34+ and CD34+/Flk-1- cells, respectively; $P < 0.05$, $n = 6$).

Transplantation of CD34+ cells and poststroke functional recovery. Stroke causes motor deficits and behavioral abnormalities (15). Dysfunction of the cortex is closely linked to disinhibition of behavior (16). Compared with sham-operated controls, mice that received CD34- cells or PBS displayed significant behavioral abnormalities on day 90 after cell transplantation ($n = 12$, for each group). Rearing counts under lighted conditions were 8.4 ± 0.8 (PBS), 8.7 ± 0.5 (CD34- cells), 4.2 ± 0.5 (CD34+ cells), and 3.0 ± 0.5 (sham-operated controls) for each of the groups. Counts of locomotion were 5.1 ± 0.4 (PBS), 5.0 ± 0.4 (CD34- cells), 3.7 ± 0.4 (CD34+ cells), and 3.3 ± 0.4 (sham). ANOVA revealed hyperactivity with respect to both rearing ($P < 0.01$) and locomotion ($P < 0.01$) in the CD34- cell- and PBS-treated groups, compared with sham-operated controls. In contrast, mice treated with CD34+ cells showed no significant hyperactivity compared with sham-operated controls ($P > 0.05$), and displayed significant improvement in both behavioral tests compared with animals that received PBS or CD34- cells ($P < 0.05$). Mice treated with CD34- cells or PBS after stroke showed loss of this "dark" response, with respect to rearing ($P > 0.05$) and locomotion ($P > 0.05$). In contrast, animals treated with CD34+ cells displayed the expected increase in rearing and locomotion in the darkness ($P < 0.01$).

Using another behavioral paradigm, excessive startle consequent to auditory stimulation was observed in poststroke animals treated with CD34- cells and PBS. Startle amplitudes were 0.9 ± 0.1 volts (PBS), 0.8 ± 0.1 (CD34- cells), 0.5 ± 0.1 (CD34+

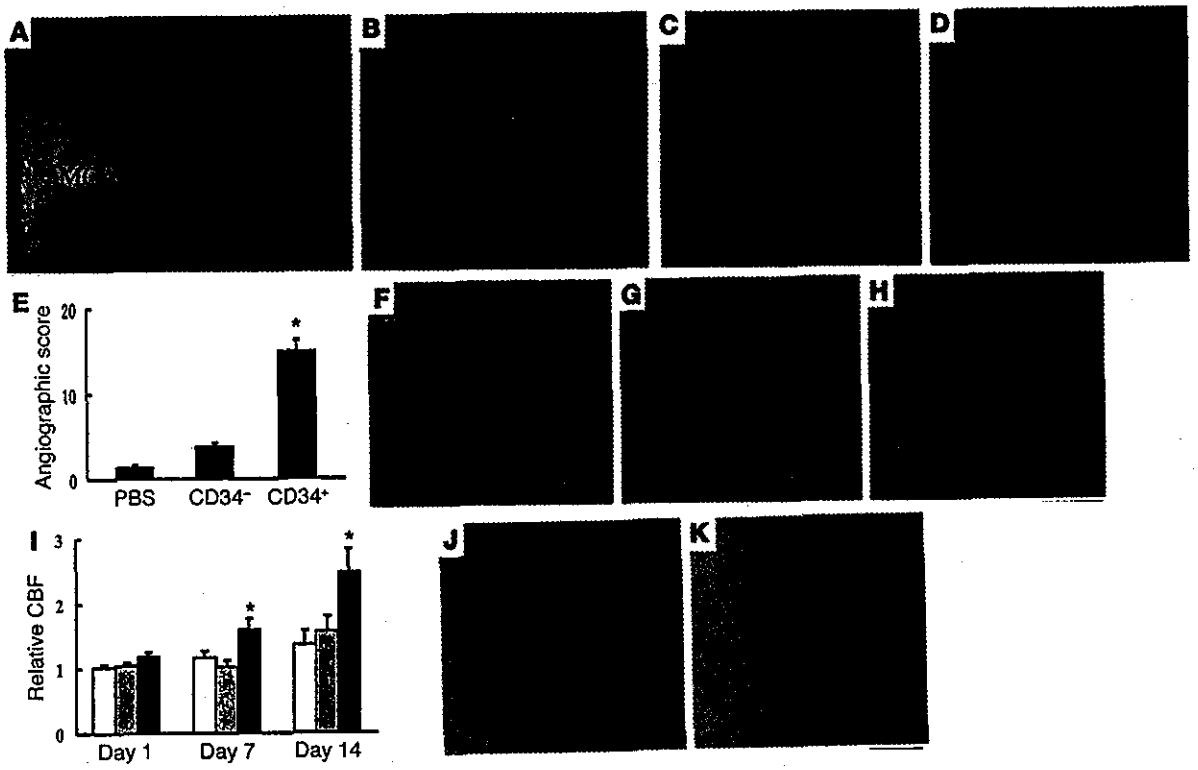

Figure 2
Transplantation of CD34⁺ cells after stroke accelerates neovascularization. (**A–D**) Mice subjected to stroke received CD34⁺ cells (**A** and **B**), CD34⁻ cells (**C**), or PBS alone (**D**) on day 2. Animals were infused with carbon black ink and killed at 24 hours after cell transplantations. Sections were stained with TTC. Neovascularization was noted at the border zone between the ACA and MCA areas (arrowheads show microvessels), especially in animals treated with CD34⁺ cells compared with those receiving CD34⁻ cells or PBS alone. (**E**) An angiographic score for each experimental condition based on analysis of 6 mice per group. (**F–H**) Activated endothelial cells were observed with antibody specific for mouse CD13 in the ACA area. **F**: CD34⁺ cells; **G**: CD34⁻ cells; **H**: PBS. (**I**) CBF was measured in the MCA area just outside of the penumbra, and values in animals treated with CD34⁺ cells (black bars), CD34⁻ cells (gray bars), or PBS (white bars) were compared with values before cell transplantation at times corresponding to days 1, 7, and 14 after cell transplantation (n = 6 per group). Data shown are relative CBF versus day the measurement was performed. (**J** and **K**) Labeling vasculature by infusion of carbon black ink demonstrated neovasculature at the border of the MCA and ACA cortex in animals treated with CD34⁺ cells (**J**) and CD34⁺/Flk-1⁻ cells (**K**) on day 7 after cell transplantation. Scale bars: 0.5 mm (**A**) and 0.1 mm (**B**, **F**, and **J**). *P < 0.05 versus PBS.

cells), and 0.4 ± 0.1 (sham) on day 90. ANOVA revealed hyperactivity in the CD34⁻ cell- and PBS-treated groups, compared with sham-operated controls (P < 0.05). In contrast, mice treated with CD34⁺ cells showed no significant hyperactivity compared with sham-operated controls (P > 0.05). Shortening of the latency period with fear conditioning was also observed in poststroke animals treated with CD34⁻ cells and PBS compared with sham-operated controls (P < 0.05). In contrast, mice treated with CD34⁺ cells showed no significant hyperactivity (P > 0.05). Similar behavioral abnormalities were also observed on day 35 after cell transplantation. Since ischemic injury in our stroke model was limited to the cortex (hippocampus and striatum were intact), it was not surprising that spatial learning (water maze testing) and passive avoidance remained unchanged and comparable in all groups when assessed 5 weeks after stroke (data not shown). Mice showed rapid recovery from focal motor deficits, and by day 16 after stroke no motor deficits were detected using a modified three-point scale (17) (data not shown).

Effect of poststroke CD34⁺ cell transplantation on endogenous neurogenesis and cortical expansion. These results suggested that cortical function and neoangiogenesis, potentially supporting integrity of the MCA cortex, might be better maintained in animals treated with CD34⁺ cells after stroke. Such maintenance of cortical integrity might reflect CD34⁺ cell–mediated enhancement of the survival of ischemic neurons or acceleration of endogenous neurogenesis. Representative brains from poststroke animals in each group (treated with PBS alone, CD34⁻ cells, or CD34⁺ cells) are shown in Figure 3, A–F. There was a prominent increase in cortical width index in animals receiving CD34⁺ cells at 14, 35, and 90 days after cell transplantation (Figure 3G). Thus, cortical expansion in animals treated with CD34⁺ cells was most likely to reflect the result of ongoing neurogenesis, rather than maintenance of the integrity of ischemic neurons from the time of induction of stroke.

Cell trace analysis with a fluorescent dye revealed that labeled transplanted CD34⁺ cells were not co-stained with antibody to a neuronal (neuron-specific nuclear protein; NeuN) or an astrocyte (glial fibrillary acidic protein) marker (not shown). However, activation of endogenous neurogenesis was observed after stroke, and this was accentuated in mice receiving CD34⁺ cells. On day 7 after administration of CD34⁺ cells, cells expressing the polysialylated neuronal cell adhesion molecule (PSA-NCAM), a marker of migrating neuronal progenitor cells (NPCs) (18), were observed in the subventricular zone (SVZ), and migration of these NPCs toward the ischemic zone was visualized on day 14 using markers

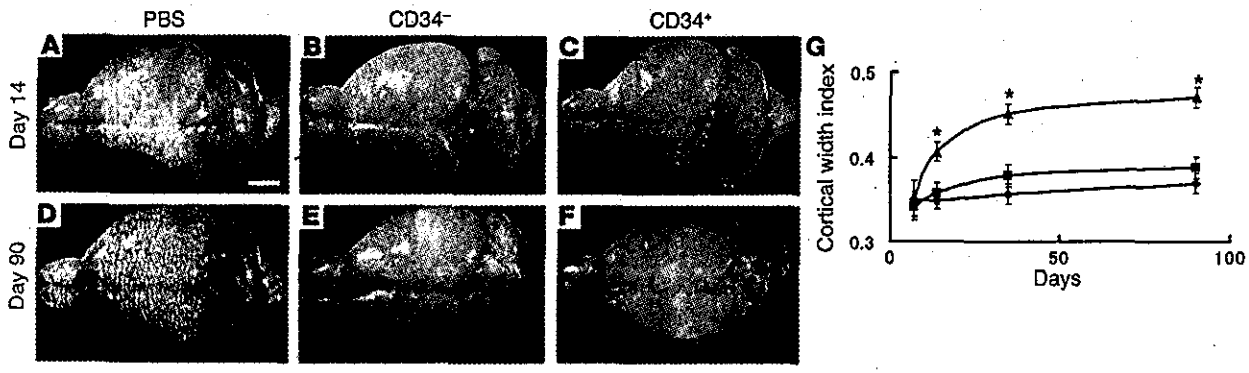

Figure 3
CD34⁺ cell transplantation induces cortical expansion after stroke. (**A–F**) On day 14 (**A–C**), and day 90 (**D–F**) after cell transplantation, the brains of mice were evaluated grossly. Compared with poststroke mice treated with PBS (**A** and **D**) or infused with CD34⁻ cells (**B** and **E**), animals transplanted with CD34⁺ cells (**C** and **F**) showed an increase in area occupied by the left cortex. (**G**) Cortical regeneration was induced by CD34⁺ cells transplantation: triangles, CD34⁺ cells; squares, CD34⁻ cells; diamonds, PBS. In each case, there were 6 animals per group. Scale bar: 2 mm (**A**). *$P < 0.05$ versus PBS.

for PSA-NCAM (Figure 4, A and B, corresponding to lower and higher magnifications, respectively), as well as the neuronal stem cell marker, Musashi-1 (Figure 4C) (19). Expression of doublecortin (DCX), a marker of immature, or early, neurons (20), was principally restricted to NPCs close to the SVZ (Figure 4D). In contrast, expression of a neuronal cell marker, NeuN, was observed after cell migration from the SVZ and appeared as a signal of lower intensity compared with nearby mature neurons (Figure 4E). The situation was quite different on the contralateral side in poststroke animals treated with CD34⁺ cells; no such movement of precursors (PSA-NCAM⁺ cells) was observed (Figure 4F). Although migrating NPCs were also seen in poststroke animals treated with PBS (Figure 4G) and CD34⁻ cells, this finding was considerably magnified in mice receiving CD34⁺ cells (Figure 4H).

To investigate mechanisms underlying cortical expansion, immunohistological analysis was conducted to visualize PSA-NCAM, NeuN, and MAP-2. On day 14 after transplantation of CD34⁻ cells after stroke, mature cortical neurons displaying neuronal markers NeuN (Figure 5A) and MAP-2 (Figure 5B) were observed up to the periphery of the ischemic area, whereas only a thin layer of migrating PSA-NCAM⁺ NPCs was observed at the ischemic edge (Figure 5C). In contrast, transplantation of CD34⁺ cells after stroke expanded cortical areas displaying a low density of NeuN⁺ (Figure 5D) and MAP-2⁺ cells (Figure 5E) beyond the boundary demarcating mature neurons. Migration of NPCs into this expanded area was also observed by PSA-NCAM staining (Figure 5F).

Next, we investigated the fate of NPCs migrating from the SVZ to the ischemic area. Poststroke animals treated with CD34⁻ cells displayed many cells with TUNEL⁺ nuclei around the lower part of cortical ischemic edge (Figure 5G). In contrast, there were a minimal number of TUNEL⁺ nuclei observed in the same region in animals subject to transplantation of CD34⁺ cells after stroke (Figure 5, H and I). Thus, animals treated with CD34⁺ cells after stroke display migration and survival of NPCs, which eventually contribute to a population of more mature neurons.

To confirm this evidence of neurogenesis, animals transplanted with CD34⁺ cells, CD34⁻ cells, or PBS after stroke were infused with

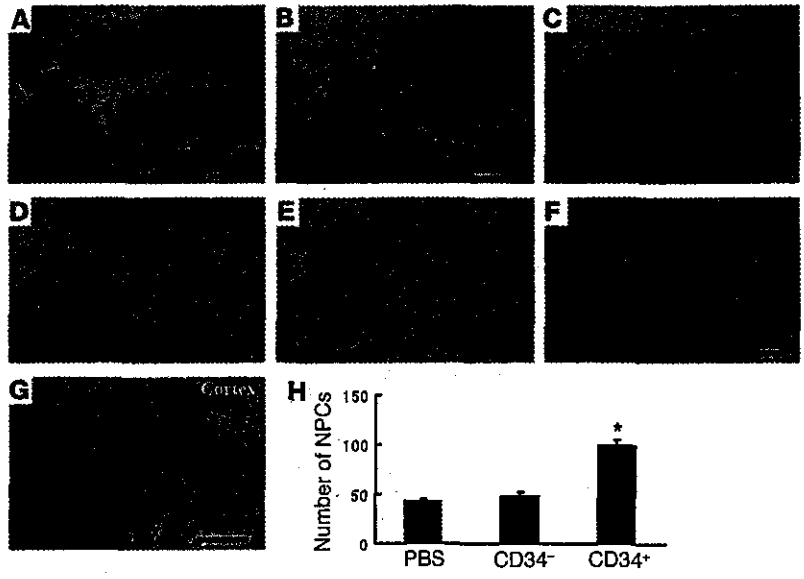

Figure 4
CD34⁺ cell transplantation accelerates neuronal regeneration after stroke. (**A** and **B**) On day 14, animals receiving CD34⁺ cells after stroke displayed migration of NPCs toward the ischemic area by PSA-NCAM immunostaining. (**C–E**) Analysis of serial sections displayed expression of neuronal stem cell markers, Musashi-1 (**C**) and DCX (**D**). Note that expression of DCX was limited to the area proximal to the SVZ. PSA-NCAM⁺ NPCs also expressed NeuN (**E**). Small NeuN⁺ nuclei were observed in PSA-NCAM⁺ NPCs, whereas more intensely staining and larger nuclei represent mature neurons. (**F**) On day 14 on the contralateral side, PSA-NCAM⁺ NPCs were limited to the SVZ; that is, no migration of NPCs was observed. (**G**) Migration of NPCs with small NeuN⁺ nuclei toward cortex was observed in poststroke mice treated with PBS on day 14 after cell transplantation. (**H**) The average number of NPCs in the white matter at the lower left of the left cortex per HPF from 5 animals under each condition. Three sections were evaluated in each animal, and $n = 5$ per group. Arrowheads delineate individual NPCs or demarcate areas rich in NPCs. Scale bars: 1 mm (**A**), 0.2 mm (**B** and **F**), and 0.4 mm (**G**). *$P < 0.05$ versus PBS.

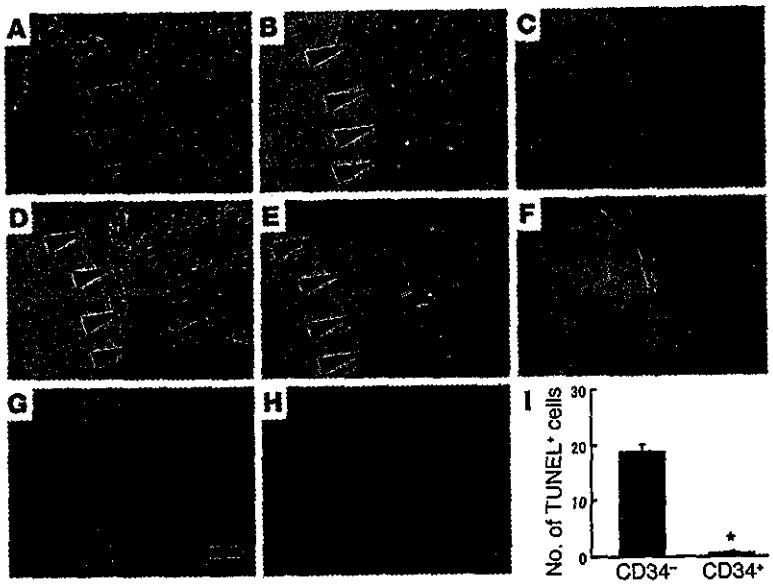

Figure 5
Therapeutic neovascularization, due to CD34+ cell transplantation after stroke, enhances neurogenesis. (**A–F**) On day 14 after CD34- cell transplantation, mature cortical neurons were observed up to the edge of the ischemic region displaying neuronal markers, NeuN (**A**) and MAP-2 (**B**), whereas only a thin layer of migrating PSA-NCAM+ NPCs was observed at the ischemic edge (**C**). In contrast, after transplantation of CD34+ cells, expanded cortical areas displaying a low density of NeuN+ (**D**) and MAP-2+ cells (**E**) were observed beyond the boundary demarcating mature neurons. Migration of NPCs into this expanded area was also observed by PSA-NCAM staining (**F**). (**G–I**) On day 14, TUNEL+ cells were visualized around the lower part of the expanded cortical area. Whereas massive cell death was observed in animals receiving CD34- cell transplantation (**G**), the number of TUNEL+ profiles was strongly reduced in mice transplanted with CD34+ cells (**H**). (**I**) The average number of TUNEL+ cells per HPF. Three sections were evaluated in each animal; $n = 5$ per group. Arrowheads indicate the expanded cortical areas displaying a low density of indicated marker. Scale bars: 100 μm (**A**) and 50 μm (**G**). *$P < 0.05$ for CD34+ versus CD34- cell transplantation.

BrdU every second day for a total of 14 days and then killed. BrdU- and NeuN-bearing cell populations were visualized to determine if a group of neurons might be undergoing cell division. In animals treated with PBS alone (Figure 6A) or CD34- cells (Figure 6B), double staining for BrdU and NeuN displayed little evidence of cells (i.e., nuclei) expressing both markers. Only in animals infused with CD34+ cells after stroke did we consistently observe double-labeled cell profiles with BrdU and NeuN to produce a merged image with cells displaying both markers (Figure 6C). Quantification of these results showed a significant increase in double-positive profiles (i.e., cells co-staining with antibody to BrdU and NeuN) in poststroke animals infused with CD34+ cells (Figure 6D). Consistent with these data, total neuronal counts (Figure 6E) from sections stained with NeuN in the left cortex 90 days after cell transplantation demonstrated a significant increase in the number of cells visualized in animals transplanted with CD34+ cells compared with those receiving CD34- cells or PBS. In addition, vasculature was visualized in the ischemic zone of the forebrain of animals treated with CD34+ cells 90 days later using anti-mouse CD31 as a marker. A distinct vascular network was seen in the expanded cortex associated with neurogenesis after stroke (Figure 6F). Such vessels displayed a pattern quite distinct from that observed on the contralateral (nonischemic) side (Figure 6G). In these vessels on the ischemic side, some endothelial cells were observed to express human CD31 antigen (Figure 6H). On day 90, mature MAP-2+ dendrites were observed in the expanded cortex of poststroke animals treated with CD34+ cells (data not shown). These data are consistent with the formation of a stable neovasculature to support regeneration of cortical neurons.

Inhibition and acceleration of angiogenesis by antiangiogenic and angiogenic agents. To investigate the hypothesis that neovascularization is essential to support endogenous neuronal regeneration, we used an antiangiogenic agent, Endostatin. The latter is known to inhibit proliferation of endothelial cells (21) and to have a direct inhibitory effect on EPCs (22). Mice were subjected to stroke, CD34+ or CD34- cells were administered, and animals were divided into two groups; one group received Endostatin and the other PBS ($n = 5$, for each group). On day 7 after cell transplantation, treatment with Endostatin suppressed endothelial proliferation to 18% ± 3% and 22% ± 3% in mice transplanted with CD34- cells and CD34+ cells, respectively, compared with proliferation observed in PBS-treated controls. Administration of Endostatin also impaired cortical expansion due to transplantation of CD34+ cells. On day 14, the cortical width index was 0.33 ± 0.01 and 0.41 ± 0.01 with and without Endostatin, respectively ($P < 0.01$). Animals treated with CD34+ cells and Endostatin after stroke displayed a reduction in migrating NPCs; 101 ± 7 cells per high-power field (HPF), for animals treated with CD34+ cells + PBS, and 21 ± 2 cells/HPF for animals treated with CD34+ cells + Endostatin ($P < 0.01$). Similarly, on day 14, the number of neurons in the poststroke cortex was less in mice treated with CD34+ cells + Endostatin (1,469 ± 53), compared with animals treated with CD34+ cells + PBS (2,213 ± 36; $P < 0.01$).

To gain further support for our hypothesis, we used the proangiogenic agent erythropoietin (EPO). EPO, well known for its essential role in regulating proliferation and differentiation of erythroid cells, has recently been found to promote mobilization of EPCs (23) and to have angiogenic potential (24). On day 4 after stroke, a significant increase in circulating CD34+ cells was observed with EPO injection (5,244 ± 1,267 and 1,333 ± 389 cells/ml in the EPO and PBS groups, respectively; $n = 6$ per group, $P < 0.05$). In addition, mice treated with EPO displayed enhanced neovascularization based on angiographic score (5.4 ± 0.8 and 1.2 ± 0.4, in EPO and PBS groups, respectively; $n = 5$ per group, $P < 0.05$). On day 28 after stroke, treatment with EPO increased the number of cells co-staining for BrdU and NeuN (3.4 ± 0.3 and 0.4 ±0.1/HPF in the EPO and PBS groups, respectively; $n = 5$ per group, $P < 0.05$). It should be noted that the magnitude of the stimulatory effect of EPO treatment on angiogenesis and neurogenesis in these experiments was less than that observed in studies with CD34+ cell transplantation, probably because of the greater number of cells transferred in the latter case.

Neurogenesis in 24-week-old mice. To analyze the effect of increased age on accelerated neurogenesis associated with CD34+ cell transplantation, 24-week-old SCID mice were used. Compared with poststroke mice treated with CD34- cells (Figure 7A), transplantation of CD34+ cells (Figure 7B) showed a significant increase in area occupied by the left cortex on day 35 (Figure 7C). In addi-

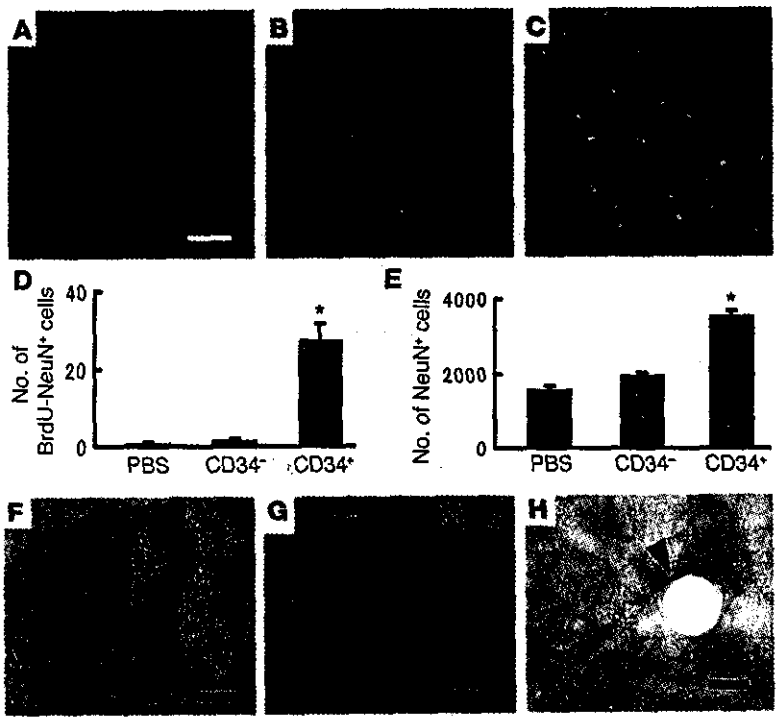

Figure 6
Therapeutic neovascularization supports survival of regenerating neurons. (**A–C**) Animals treated with PBS alone (**A**), CD34⁻ cells (**B**), or CD34⁺ cells (**C**) were infused with BrdU, killed, and studied immunohistochemically with antibody to BrdU (red), NeuN (green), or both (yellow). (**D**) The average number of double-positive cells (stained with antibody to BrdU and NeuN) per HPF on day 90 after cell transplantation. Ten fields were evaluated in each animal, and $n = 6$ per group. $^*P < 0.05$ versus PBS. (**E**) On day 90 after cell transplantation, brain sections from animals treated with PBS alone, CD34⁻ cells, or CD34⁺ cells were stained with antibody to NeuN, and the number of total neurons in the left cortex was counted. (**E**) The average number of total NeuN⁺ cells in the left cortex. $n = 6$ per group; $^*P < 0.05$ versus PBS. (**F** and **G**) On day 90 after cell transplantation, mouse CD31 was visualized immunohistologically in forebrain sections from poststroke animals. Newly formed vascular networks were observed in the expanded cortex. The vascular pattern displayed by these neovessels on the ipsilateral (**F**, ischemic side) was different from that observed on the contralateral side (**G**). (**H**) On day 90, human CD31 was visualized immunohistologically. Human endothelial cells were observed in the regenerating cortex of animals treated with CD34⁺ cells after stroke. The arrowhead shows a human CD31⁺ endothelial cell. Scale bars: 50 μm (**A**), 100 μm (**F** and **G**), and 20 μm (**H**).

tion, evidence of vascular activation, as judged by reactivity with anti-CD13 antibody, was observed in mice treated with CD34⁺ cells (Figure 7D, CD34⁻ cells; Figure 7E, CD34⁺ cells). Migration of NPCs was observed in mice treated with CD34⁻ cells (Figure 7F) and CD34⁺ cells (Figure 7G), but a significant enhancement was observed in animals receiving CD34⁺ cells (Figure 7H). Only a thin layer of migrating PSA-NCAM⁺ NPCs was observed at the ischemic edge in animals treated with CD34⁻ cells (Figure 7I). In contrast, CD34⁺ cell transplantation resulted in a much thicker layer of PSA-NCAM⁺ cells (Figure 7J). Comparing these data in 24-week-old animals with our previous results using 5-week-old mice, the older animals displayed a similar cortical width index (5 weeks old, 0.45 ± 0.01; 24 weeks old, 0.43 ± 0.02; $P > 0.05$), although older age was associated with a decrease in NPCs migrating into the cortex (5 weeks old, 71 ± 3 cells/HPF; 24 weeks old, 43 ± 4 cells/HPF; $P < 0.05$) on day 35 after CD34⁺ cell transplantation.

Discussion

Our findings show that administration of human CD34⁺ cells to immunocompromised mice 48 hours after stroke enhances neovascularization at the border of the ischemic zone followed by endogenous neurogenesis. Furthermore, suppression of the neo-

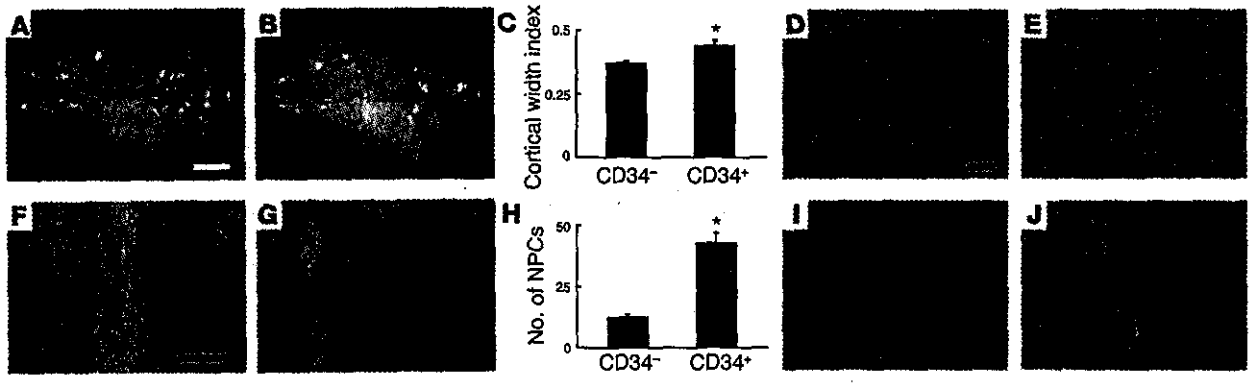

Figure 7
CD34⁺ cell transplantation in 24-week-old animals. (**A–C**) On day 35 after cell transplantation, the brains were evaluated. Compared with poststroke mice treated with CD34⁻ cells (**A**), animals transplanted with CD34⁺ cells (**B**) showed an increase in area occupied by the left cortex. Significant cortical regeneration was induced by CD34⁺ cells transplantation (**C**). (**D** and **E**) Compared with CD34⁻ cell transplantation (**D**), increased evidence of activated vasculature was observed in animals receiving CD34⁺ cells (**E**), as detected with mouse specific anti-CD13 antibody. (**F–H**) Migration of NPCs (small NeuN⁺ nuclei migrating toward the cortex) was observed in poststroke mice treated with CD34⁻ cells (**F**) and with CD34⁺ cells (**G**). However, a significant increase in migrating NPCs was induced by CD34⁺ cell transplantation (**H**). (**I** and **J**) A thin layer of migrating PSA-NCAM⁺ NPCs was observed at the ischemic edge of the cortex in animals treated with CD34⁻ cells (**I**), compared with a much thicker layer in those receiving CD34⁺ cells (**J**). Scale bars: 2 mm (**A**), 0.1 mm (**D** and **I**), and 0.4 mm (**F**). $n = 4$ in each group; $^*P < 0.05$ versus CD34⁻ cells.

vascularization by an antiangiogenic agent impaired neurogenesis. On the basis of these data, accelerated neovessel formation seems to be essential for enhancing endogenous neurogenesis and improving functional recovery.

The generation of new neurons in the adult is largely restricted to two regions: the SVZ lining the lateral ventricles and the subgranular zone of the dentate gyrus (25). In the transient cerebral ischemia model, evidence has been provided that neuronal regeneration occurs (10, 20). However, even in a transient ischemia model in which integrity of the microcirculation is maintained, it was shown that greater than 80% of newly formed neurons died, most likely because of unfavorable environmental conditions including lack of trophic support and exposure to products of damaged tissue. These considerations may underlie the observation that only 0.2% of nonviable ischemic neurons were replaced through neurogenesis (20). Such previous observations are consistent with our current results in animals treated with $CD34^-$ cells or PBS, in which there was no enhancement of neovascularization, no neurogenesis, and no functional recovery.

Consistent with these data, Endostatin-mediated suppression of endothelial proliferation and direct effects on EPCs abrogated the beneficial effect $CD34^+$ cells on neurogenesis and cortical expansion, and at the same time inhibited formation of neovasculature after stroke. In contrast, when EPO was used as a proangiogenic agent (recently, EPO has also been found to promote mobilization of EPCs) (23, 24), accelerated formation of neovasculature was accompanied by enhanced neurogenesis after stroke in our murine model. Our data provide the first direct link between therapeutic neovascularization after stroke and enhanced neurogenesis; formation of neovasculature after stroke supported neurogenesis. Consistent with a previous report (26), activation of NPCs after stroke was induced in adult, as well as young, murine brain. The number of activated NPCs was less in the adult animals, but a significant increase was still observed consequent to $CD34^+$ cells transplantation, with evidence of activated vasculature in brains of the older animals. These findings support our hypothesis that administration of $CD34^+$ cells provides a milieu favorable for neovascularization and endogenous neurogenesis, even in the mature brain.

A relationship between angiogenesis and neurogenesis would be consistent with regeneration of parenchymal cells in other organs subject to therapeutic angiogenesis (27, 28). Mechanisms underlying this observation might include more optimal preparation of the ischemic tissue bed for neuronal regeneration by accelerated removal of debris and toxic products, and/or the enhanced production of chemokines and trophic agents by neovasculature. Factors involved might be FGF2 (11), PDGF (29), brain-derived neurotrophic factor (30), and IL-8 (31), which have the capacity to induce mitogenesis, differentiation, recruitment, and survival of NPCs and newly generated neurons. In addition, mediators produced by $CD34^+$ cells (4), such as VEGF, FGF2, and IGF-1, have been shown to accelerate endogenous neurogenesis (10–12). The effects of these and other factors derived from $CD34^+$ cells (32, 33) acting on the vasculature are also likely to have an important role in providing an environment conducive to neurogenesis. Newly formed neurons in the setting of neovascularization have been shown to integrate into neuronal networks in adult animals (34); in fact, lack of participation of neurons in such neuronal circuits is probably associated with cell death (20). Our results provide strong support for the hypothesis that neovascularization consequent to administration of $CD34^+$ cells induces neurogenesis by providing the necessary supportive environment. Whereas perturbation of the neurovascular unit has been proposed to contribute to tissue damage in stroke, neoangiogenesis and accompanying neurogenesis could be considered to be rebuilding crucial elements of the neurovascular unit (35). Previous reports have demonstrated that endothelial cells in newly formed vessels after stroke mainly originate from pre-existing endothelial cells (due to proliferation) with a contribution of circulating EPCs (36, 37). Consistent with these findings, we observed proliferating mouse endothelial cells around the ischemic area soon after stroke. The latter endothelial cells could be visualized, at least in part, with antibody specific for human CD31, after transplantation of human $CD34^+$ cells. Furthermore, diminished neovascularization was observed after stroke following transplantation of $CD34^+/Flk\text{-}1^-$ cells, compared with $CD34^+$ cells (containing both $Flk\text{-}1^-$ and $Flk\text{-}1^+$ cells) despite similar activation of murine endothelial cells in the ischemic territory in each case. These results support potential contribution of $CD34^+/Flk\text{-}1^+$ cells (a population known to be rich in EPCs) in expansion of the vascular network after stroke.

The actual pattern of the newly formed vascular network was quite different on the ipsilateral (ischemic) from the contralateral side in poststroke mice treated with $CD34^+$ cells. This observation suggests that formation of vasculature consequent to transplantation of $CD34^+$ cells after stroke does not simply reconstitute the original vascular network. Rather, a new vascular pattern arises (a true neovasculature) that is capable of supporting neurogenesis, followed by functional recovery, even though it displays a relatively "aberrant" pattern, at least anatomically, compared with the contralateral vasculature.

Our observations provide evidence of a crucial role for neovessel formation, achieved through the administration of $CD34^+$ cells after stroke, in processes that underlie neurogenesis. These data strongly suggest that neovascularization is essential for neuronal regeneration after stroke and that therapeutic neovascularization is a potentially effective means of enhancing functional recovery. Our observations might explain the mild therapeutic effect achieved by neuronal cell transplantation after stroke reported in humans (38). This leads to the hypothesis that therapeutic neovascularization may be required to achieve optimal "take" of transplanted neuronal precursors in the setting of ischemia. Although the current data bear most directly on the endogenous neuronal response to cerebrovascular ischemia, it is possible that enhanced formation of neovasculature may also be important for survival of embryonic (39) and neural (40) stem cell transplants in other circumstances, such as neurodegenerative disorders.

Methods

All procedures were done in accordance with the National Cardiovascular Center Animal Care and Use, and Human Assurance Committees. Quantitative measurements and behavioral tests were conducted by investigators blinded to the experimental protocol and identity of the sections and animals under study.

Induction of focal cerebral ischemia. Permanent focal cerebral infarction was produced by ligation and disconnection of the distal portion of the left MCA. Male SCID mice (5 weeks old; Oriental Yeast Co. Ltd., Tokyo, Japan) were used for experiments involving human cell transplantation. Male C57BL/6J mice (24 weeks old; Clea Japan Inc., Tokyo, Japan) were used for experiments with human recombinant EPO (Kirin, Tokyo, Japan). Under halothane inhalation (3%), the left MCA was isolated, electrocauterized, and disconnected just distal to its crossing of the olfactory tract (distal M1 portion). CBF in the MCA area was monitored as described (41). Mice that showed decreased CBF by approximately 75% immediately after and 24 hours after ligation were used for our experiments (success rate of >95%). Body temperature was maintained at 36.5–37°C using a heat lamp during

the operation and for 2 hours after MCA occlusion. The ratio of CBF after cell transplantation to CBF before cell transplantation was calculated to evaluate the change of CBF (termed relative CBF).

Analysis of perfusion and brain infarction after MCA occlusion. Carbon black ink (Fuekinori Kogyo Co. Ltd., Osaka, Japan) was used to delineate the perfused area after MCA ligation as described (42). Viability of brain tissue was evaluated using TTC (Sigma-Aldrich, St. Louis, Missouri, USA). Coronal sections (1 mm thick) of the forebrain were stained with 1% TTC, and the images of sections from the exact center of the forebrain were captured using a microscopic digital camera system (Olympus, Tokyo, Japan). The width of viable cortex was determined by NIH image.

Administration of $CD34^+$ cells after stroke. $CD34^+$ cells (containing $Flk\text{-}1^-$ and $Flk\text{-}1^+$ cell populations) and $CD34^+/Flk\text{-}1^-$ cells were isolated from cord blood using a Direct CD34 Progenitor Cell Isolation kit (Miltenyi Biotec, Bergisch Gladbach, Germany), CD34 Multisort kit (Miltenyi Biotec), and anti-Flk-1 antibody (Sigma-Aldrich), according to the manufacturers' protocols. $CD34^-$ mononuclear cells were also collected for control experiments. In each case, cell populations were analyzed by FACS (BD Biosciences, San Jose, California, USA) using PerCP-conjugated anti-CD34 antibody (BD Biosciences), phycoerythrin-conjugated (PE-conjugated) anti-P1H12 antibody (BD Biosciences), and anti-Flk-1 antibody (Sigma-Aldrich) conjugated with FITC according to the manufacturer's protocol (Zenon Alexa Fluor; Molecular Probes Inc., Eugene, Oregon, USA). For labeling studies, cells were incubated with the fluorescent dye chloromethylbenzamido (CM-DiI; Molecular Probes Inc.). Forty-eight hours after stroke, 5×10^5 $CD34^+$, $CD34^+/FLK\text{-}1^-$, $CD34^-$ cells, or the same volume (100 μl) of PBS were infused intravenously via the tail vein.

For the analysis of the effect of aging on neurogenesis, 24-week-old male SCID mice were used. Because of the known increased evidence of tumors, infection (for example, excess mucus in the eye), and elevated plasma immunoglobulins in older SCID mice, the presence of each of these conditions was also investigated. Mice with evidence of weight loss, tumors, infection, or elevated plasma immunoglobulins (> 10 μg/ml) were excluded from further analysis.

Immunohistochemistry. Mice brains were removed and fixed in paraformaldehyde. Coronal sections (20 μm) were prepared using a vibratome (Leica Microsystems Inc., Wetzlar, Germany). To assess cell proliferation and angiogenesis, fresh frozen sections (20 μm) were prepared and fixed in acetone. Sections were subjected to immunohistochemistry with antibody to NeuN (Chemicon International, Temecula, California, USA), mouse-specific antibody to CD31 (BD Biosciences), human-specific antibody to CD31 (DAKO A/S, Glostrup, Denmark), mouse-specific antibody to CD13 (Santa Cruz Biotechnology, Santa Cruz, California, USA), and antibodies to MAP-2 (Sigma-Aldrich), human von Willebrand Factor (DAKO A/S), PSA-NCAM (Chemicon International), DCX (Chemicon International), Musashi-1 (19), TUNEL (Molecular Probes Inc.), or BrdU (Boehringer Ingelheim, Ingelheim, Germany).

Cell proliferation analysis. For assessment of cell proliferation in vivo, BrdU (Sigma-Aldrich) was administered intraperitoneally. In the case of endothelial cell proliferation, BrdU (200 mg/kg) was administered 24 hours before killing. For endogenous neurogenesis, 50 mg/kg of BrdU was injected every second day for a total of 14 days. Cells co-staining for BrdU and mouse-specific antibody to CD31 using confocal microscopy (Olympus) in HPFs (×40 of objective lens) were counted as proliferating endothelial cells. The cell population co-staining for BrdU and NeuN was counted as regenerating-proliferating neurons. For quantitative analysis, brain sections at the exact center of the forebrain were stained, and the left cortical area of 1 mm (or > 1 mm) distal from the midline was examined by two investigators blinded to the experimental protocol. In each case, 10 representative fields were evaluated before quantitative results were analyzed.

Assessment of angiogenesis. For assessment of angiogenesis at the border of MCA and ACA areas, carbon black perfusion was used to visualize the vasculature and TTC staining to demarcate the border of viable and non-viable tissue. Semi-quantitative analysis of angiogenesis made use of the angiographic score and was calculated by a previously described method (43). Microscopic digital images were scanned into a computer (Olympus), and an overlay, composed of 50-μm-diameter circles arranged in rows spaced 100 μm apart, was superimposed on the image. The total number of grids intersecting the border zone containing a microvessel was counted. Mouse-specific antibody to CD13 was used to visualize 'activated' vasculature.

Assessment of ischemic brain damage and neurogenesis. For determination of the cortical width index, whole-brain images were captured using a microscopic digital camera system (Olympus). The width at the midpoint of the forebrain was measured, and the ratio of left width to right width was defined as the cortical width index. To quantify accelerated neurogenesis, three brain sections around the center of the forebrain on day 14 after cell transplantation were stained with NeuN or TUNEL. The number of small NeuN nuclei-positive cells in the white matter at lower left of the left cortex and the number of $TUNEL^+$ cells around the lower part of ischemic cortical edge was counted in HPFs. For determining the number of neurons in the left cortex, brain sections of the exact center of the forebrain on day 90 were stained with NeuN, and the total number of $NeuN^+$ cells was quantitated.

Behavioral analysis. To assess cortical function, mice were subjected to behavioral testing in the open-field task (44) on day 35 or 90 after cell transplantation. Auditory startling behavior was tested as described (45). To estimate learning activity, mice were tested by water maze test (46) and passive avoidance test (47). To exclude the contribution of physical deficits directly related to the operative procedure and induction of stroke, motor deficiencies were examined on days 9 and 16 after stroke. Neurological deficits were scored on a three-point modified scale as described (17). Body weight, monitored in each experimental group, displayed no significant differences (data not shown).

Inhibition and promotion of neovascularization. Inhibition of neovascularization was achieved by administering Endostatin (10 μg; subcutaneous; Calbiochem-Novabiochem, Darmstadt, Germany) once daily for 14 days. To stimulate mobilization of EPCs originating in the host, EPO (1,000 μg/kg) was injected subcutaneously 24, 48, and 72 hours after ischemia. Peripheral blood cells were analyzed using FITC-conjugated anti-mouse CD45 (BD Biosciences), PE-conjugated anti-mouse CD34 antibodies (BD Biosciences), and 7-amino-actinomycin D viability Dye (Beckman Coulter Inc., Marseille Cedex, France), as described (48), using counting beads (BD Biosciences) as an internal control.

Data analysis. In all experiments, mean ± SE is reported. Statistical comparisons among groups were determined using one-way ANOVA. Where indicated, individual comparisons were performed using Student's *t* test.

Acknowledgments

Musashi-1 was generously provided by H. Okano at Keiou University in Japan. This work was partially supported by the Uehara, Takeda, and Terumo Medical Foundations, Grant-in-Aid for Scientific Research from the ministry of Education (15590785) and from the Ministry of Health, Labour, and Welfare (16C-7, H16-CK-004). We would like to thank Y. Kasahara, K. Obata, and Y. Okinaka for technical assistance.

Received for publication November 24, 2003, and accepted in revised form May 18, 2004.

Address correspondence to: Akihiko Taguchi, Department of Cerebrovascular Disease, National Cardiovascular Center, 5-7-1 Fujishiro-dai, Suita, Osaka 565-8565, Japan. Phone: 81-6-6833-5012; Fax: 81-6-6872-7485; E-mail: ataguchi@res.ncvc.go.jp.

1. Asahara, T., et al. 1997. Isolation of putative progenitor endothelial cells for angiogenesis. *Science.* 275:964–967.
2. Asahara, T., et al. 1999. Bone marrow origin of endothelial progenitor cells responsible for postnatal vasculogenesis in physiological and pathological neovascularization. *Circ. Res.* 85:221–228.
3. Kawamoto, A., et al. 2001. Therapeutic potential of ex vivo expanded endothelial progenitor cells for myocardial ischemia. *Circulation.* 103:634–637.
4. Majka, M., et al. 2001. Numerous growth factors, cytokines, and chemokines are secreted by human CD34$^+$ cells, myeloblasts, erythroblasts, and megakaryoblasts and regulate normal hematopoiesis in an autocrine/paracrine manner. *Blood.* 97:3075–3085.
5. Taguchi, A., Ohtani, M., Soma, T., Watanabe, M., and Kinosita, N. 2003. Therapeutic angiogenesis by autologous bone-marrow transplantation in a general hospital setting. *Eur. J. Vasc. Endovasc. Surg.* 25:276–278.
6. Tateishi-Yuyama, E., et al. 2002. Therapeutic angiogenesis for patients with limb ischaemia by autologous transplantation of bone-marrow cells: a pilot study and a randomised controlled trial. *Lancet.* 360:427–435.
7. Hamano, K., et al. 2001. Local implantation of autologous bone marrow cells for therapeutic angiogenesis in patients with ischemic heart disease: clinical trial and preliminary results. *Jpn. Circ. J.* 65:845–847.
8. Chen, J., et al. 2001. Intravenous administration of human umbilical cord blood reduces behavioral deficits after stroke in rats. *Stroke.* 32:2682–2688.
9. Hess, D.C., et al. 2002. Bone marrow as a source of endothelial cells and NeuN-expressing cells after stroke. *Stroke.* 33:1362–1368.
10. Nakatomi, H., et al. 2002. Regeneration of hippocampal pyramidal neurons after ischemic brain injury by recruitment of endogenous neural progenitors. *Cell.* 110:429–441.
11. Drago, J., Murphy, M., Carroll, S.M., Harvey, R.P., and Bartlett, P.F. 1991. Fibroblast growth factor-mediated proliferation of central nervous system precursors depends on endogenous production of insulin-like growth factor I. *Proc. Natl. Acad. Sci. U. S. A.* 88:2199–2203.
12. Jin, K., et al. 2002. Vascular endothelial growth factor (VEGF) stimulates neurogenesis in vitro and in vivo. *Proc. Natl. Acad. Sci. U. S. A.* 99:11946–11950.
13. Solovey, A., et al. 1997. Circulating activated endothelial cells in sickle cell anemia. *N. Engl. J. Med.* 337:1584–1590.
14. Bhagwat, S.V., Petrovic, N., Okamoto, Y., and Shapiro, L.H. 2003. The angiogenic regulator CD13/APN is a transcriptional target of Ras signaling pathways in endothelial morphogenesis. *Blood.* 101:1818–1826.
15. Van Dam, D., et al. 2003. Age-dependent cognitive decline in the APP23 model precedes amyloid deposition. *Eur. J. Neurosci.* 17:388–396.
16. Farkas, T., et al. 2003. Peripheral nerve injury influences the disinhibition induced by focal ischaemia in the rat motor cortex. *Neurosci. Lett.* 342:49–52.
17. Tamatani, M., et al. 2001. ORP150 protects against hypoxia/ischemia-induced neuronal death. *Nat. Med.* 7:317–323.
18. Iwai, M., et al. 2003. Temporal profile of stem cell division, migration, and differentiation from subventricular zone to olfactory bulb after transient forebrain ischemia in gerbils. *J. Cereb. Blood Flow Metab.* 23:331–341.
19. Sakakibara, S., et al. 1996. Mouse-Musashi-1, a neural RNA-binding protein highly enriched in the mammalian CNS stem cell. *Dev. Biol.* 176:230–242.
20. Arvidsson, A., Collin, T., Kirik, D., Kokaia, Z., and Lindvall, O. 2002. Neuronal replacement from endogenous precursors in the adult brain after stroke. *Nat. Med.* 8:963–970.
21. O'Reilly, M.S., et al. 1997. Endostatin: an endogenous inhibitor of angiogenesis and tumor growth. *Cell.* 88:277–285.
22. Capillo, M., et al. 2003. Continuous infusion of endostatin inhibits differentiation, mobilization, and clonogenic potential of endothelial cell progenitors. *Clin. Cancer Res.* 9:377–382.
23. Bahlmann, F.H., et al. 2004. Erythropoietin regulates endothelial progenitor cells. *Blood.* 103:921–926.
24. Jaquet, K., Krause, K., Tawakol-Khodai, M., Geidel, S., and Kuck, K.H. 2002. Erythropoietin and VEGF exhibit equal angiogenic potential. *Microvasc. Res.* 64:326–333.
25. Gage, F.H. 2000. Mammalian neural stem cells. *Science.* 287:1433–1438.
26. Yagita, Y., et al. 2001. Neurogenesis by progenitor cells in the ischemic adult rat hippocampus. *Stroke.* 8:1890–1896.
27. Ross, M.A., Sander, C.M., Kleeb, T.B., Watkins, S.C., and Stolz, D.B. 2001. Spatiotemporal expression of angiogenesis growth factor receptors during the revascularization of regenerating rat liver. *Hepatology.* 34:1135–1148.
28. Toda, S., et al. 1999. Immunohistochemical expression of growth factors in subacute thyroiditis and their effects on thyroid folliculogenesis and angiogenesis in collagen gel matrix culture. *J. Pathol.* 188:415–422.
29. Johe, K.K., Hazel, T.G., Muller, T., Dugich-Djordjevic, M.M., and McKay, R.D. 1996. Single factors direct the differentiation of stem cells from the fetal and adult central nervous system. *Genes Dev.* 10:3129–3140.
30. Leventhal, C., Rafii, S., Rafii, D., Shahar, A., and Goldman, S.A. 1999. Endothelial trophic support of neuronal production and recruitment from the adult mammalian subependyma. *Mol. Cell. Neurosci.* 13:450–464.
31. Araujo, D.M., and Cotman, C.W. 1993. Trophic effects of interleukin-4, -7 and -8 on hippocampal neuronal cultures: potential involvement of glial-derived factors. *Brain Res.* 600:49–55.
32. Valable, S., et al. 2003. Angiopoietin-1-induced PI3-kinase activation prevents neuronal apoptosis. *FASEB J.* 17:443–445.
33. Sun, W., Funakoshi, H., and Nakamura, T. 2002. Localization and functional role of hepatocyte growth factor (HGF) and its receptor c-met in the rat developing cerebral cortex. *Brain Res. Mol. Brain Res.* 103:36–48.
34. Louissaint, A., Jr., Rao, S., Leventhal, C., and Goldman, S.A. 2002. Coordinated interaction of neurogenesis and angiogenesis in the adult songbird brain. *Neuron.* 34:945–960.
35. Lo, E.H., Dalkara, T., and Moskowitz, M.A. 2003. Mechanisms, challenges and opportunities in stroke. *Nat. Rev. Neurosci.* 4:399–415.
36. Beck, H., et al. 2003. Participation of bone marrow-derived cells in long-term repair processes after experimental stroke. *J. Cereb. Blood Flow Metab.* 23:709–717.
37. Zhang, Z.G., Zhang, L., Jiang, Q., and Chopp, M. 2002. Bone marrow-derived endothelial progenitor cells participate in cerebral neovascularization after focal cerebral ischemia in the adult mouse. *Circ. Res.* 90:284–288.
38. Kondziolka, D., et al. 2000. Transplantation of cultured human neuronal cells for patients with stroke. *Neurology.* 55:565–569.
39. Hoehn, M., et al. 2002. Monitoring of implanted stem cell migration in vivo: a highly resolved in vivo magnetic resonance imaging investigation of experimental stroke in rat. *Proc. Natl. Acad. Sci. U. S. A.* 99:16267–16272.
40. Abe, K. 2000. Therapeutic potential of neurotrophic factors and neural stem cells against ischemic brain injury. *J. Cereb. Blood Flow Metab.* 20:1393–1408.
41. Matsushita, K., et al. 1998. Marked, sustained expression of a novel 150-kDa oxygen-regulated stress protein, in severely ischemic mouse neurons. *Brain Res. Mol. Brain Res.* 60:98–106.
42. Matsuyama, T., et al. 1983. Why are infant gerbils more resistant than adults to cerebral infarction after carotid ligation? *J. Cereb. Blood Flow Metab.* 3:381–385.
43. Takeshita, S., et al. 1994. Therapeutic angiogenesis. A single intraarterial bolus of vascular endothelial growth factor augments revascularization in a rabbit ischemic hind limb model. *J. Clin. Invest.* 93:662–670.
44. Kimble, D.P. 1968. Hippocampus and internal inhibition. *Psychol. Bull.* 70:285–295.
45. Sasaki, H., Iso, H., Coffey, P., Inoue, T., and Fukuda, Y. 1998. Prepulse facilitation of auditory startle response in hamsters. *Neurosci. Lett.* 248:117–120.
46. Balschun, D., et al. 2003. Does cAMP response element-binding protein have a pivotal role in hippocampal synaptic plasticity and hippocampus-dependent memory? *J. Neurosci.* 23:6304–6314.
47. Mereu, G., et al. 2003. Prenatal exposure to a cannabinoid agonist produces memory deficits linked to dysfunction in hippocampal long-term potentiation and glutamate release. *Proc. Natl. Acad. Sci. U. S. A.* 100:4915–4920.
48. Gratama, J.W., et al. 1999. Comparison of single- and dual-platform assay formats for CD34$^+$ haematopoietic progenitor cell enumeration. *Clin. Lab. Haematol.* 21:337–346.

Circulating CD34-Positive Cells Provide an Index of Cerebrovascular Function

Akihiko Taguchi, MD; Tomohiro Matsuyama, MD; Hiroshi Moriwaki, MD; Takuya Hayashi, MD; Kohei Hayashida, MD; Kazuyuki Nagatsuka, MD; Kenichi Todo, MD; Katsushi Mori; David M. Stern, MD; Toshihiro Soma, MD; Hiroaki Naritomi, MD

Background—Increasing evidence points to a role for circulating endothelial progenitor cells, including populations of CD34- and CD133-positive cells present in peripheral blood, in maintenance of the vasculature and neovascularization. Immature populations, including CD34-positive cells, have been shown to contribute to vascular homeostasis, not only as a pool of endothelial progenitor cells but also as a source of growth/angiogenesis factors at ischemic loci. We hypothesized that diminished numbers of circulating immature cells might impair such physiological and reparative processes, potentially contributing to cerebrovascular dysfunction.

Methods and Results—The level of circulating immature cells, CD34-, CD133-, CD117-, and CD135-positive cells, in patients with a history of atherothrombotic cerebral ischemic events was analyzed to assess possible correlations with the degree of carotid atherosclerosis and number of cerebral infarctions. There was a strong inverse correlation between numbers of circulating CD34- and CD133-positive cells and cerebral infarction. In contrast, there was no correlation between the degree of atherosclerosis and populations of circulating immature cells. Analysis of patients with cerebral artery occlusion revealed a significant positive correlation between circulating CD34- and CD133-positive cells and regional blood flow in areas of chronic hypoperfusion.

Conclusions—These results suggest a possible contribution of circulating CD34- and CD133-positive cells in maintenance of the cerebral circulation in settings of ischemic stress. Our data demonstrate the utility of a simple and precise method to quantify circulating CD34-positive cells, the latter providing a marker of cerebrovascular function. (***Circulation.* 2004;109:2972-2975.)**

Key Words: cerebral infarction ■ cerebral ischemia ■ antigens, CD34 ■ stem cells

Although it had traditionally been assumed that replacement of damaged endothelium resulted only from outgrowth of preexisting vasculature, recent studies have identified endothelial progenitor cells (EPCs) that appear to contribute to vascular homeostasis and repair.[1] Clinical trials to assess the therapeutic potential of bone marrow–derived mononuclear cells, a rich source of immature cells including EPCs, in hind-limb[2,3] and cardiac ischemia[4] have been initiated and have, thus far, provided promising results. Furthermore, immature cells, including CD34-positive ($CD34^+$) cells, have been shown to contribute to maintenance of the vasculature, not only as a pool of EPCs but also as the source of growth/angiogenesis factors.[5] Bone marrow–derived immature cells have also been shown to participate in neovascularization of ischemic brain after experimental stroke.[6] On the basis of these results, we hypothesized that levels of circulating immature cells might be proportional to the resilience of the cerebral circulation to ischemic stress; ie, lower numbers of circulating immature cells might be associated with cerebral ischemia and infarction.

Methods

The institutional review board of the National Cardiovascular Center approved this study. All subjects provided informed consent. Circulating $CD34^+$ cells in 50 μL of peripheral blood were quantified according to the manufacturer's protocol (ProCOUNT, Becton Dickinson Biosciences). To minimize intersample variation for measurements of $CD34^+$ cells, several methods were used: A nucleic acid dye was added as a threshold reagent; a no-wash technique was performed to eliminate cell loss, and reverse pipetting was used; an internal reference particle was added for determination of absolute cell numbers; and an isotype control, matched for the concentration of anti-CD34 antibody and fluorochrome-to-protein ratio, was included. All measurements were performed in triplicate (Figure 1A, control; Figure 1B, CD34). To quantify other stem cell populations (besides $CD34^+$ cells), immature mononuclear cells were enriched

Received December 8, 2003; de novo received April 12, 2004; accepted May 11, 2004.

From the Departments of Cerebrovascular Disease (A.T., H.M., K.N., K.T., H.N.), Radiology and Nuclear Medicine (T.H., K.H.), and Clinical Physiology (K.M.), National Cardiovascular Center, Osaka, Japan; Department of Internal Medicine (T.M.), Hyogo College of Medicine, Hyogo, Japan; Dean's Office (D.M.S.), Medical College of Georgia, Augusta, Ga; and Department of Hematology (T.S.), Osaka Minami National Hospital, Osaka, Japan.

Correspondence to Akihiko Taguchi, Department of Cerebrovascular Disease, National Cardiovascular Center, 5-7-1 Fujishiro-dai, Suita, Osaka, 565-8565 Japan. E-mail ataguchi@res.ncvc.go.jp

Circulation is available at http://www.circulationaha.org

DOI: 10.1161/01.CIR.0000133311.25587.DE

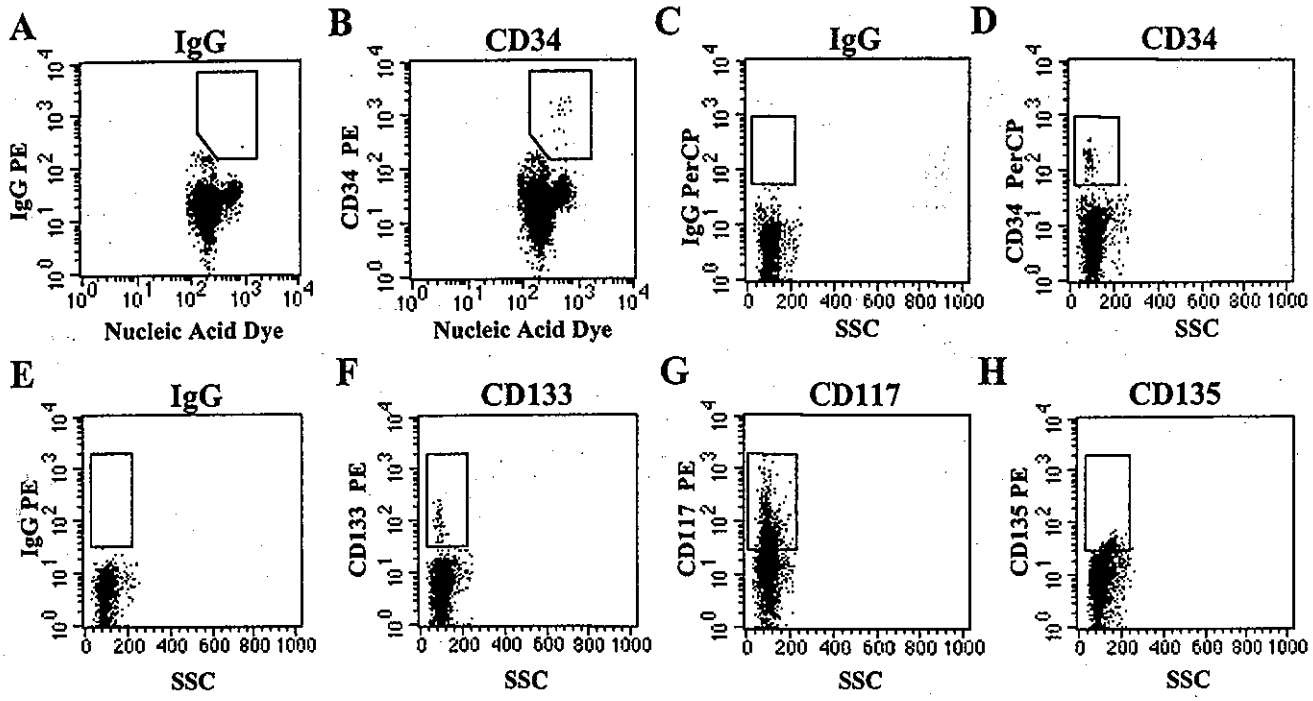

Figure 1. Quantification of circulating immature cells in patients with stroke. Nucleic acid dye versus CD34 PE dot plot was gated on lymphocytes and CD45 dim leukocytes. A, Results with an isotype-matched control antibody. B, Results with anti-CD34 antibody. Enriched immature mononuclear cells were double stained with PerCP-conjugated CD34 antibody (D) and PE-conjugated CD133 (F), CD117 (G), or CD135 (H) antibody. The number of cells in a region including brightly stained cells was counted. C and E, Staining with isotype nonimmune control antibody.

from 2 mL of peripheral blood by antibody-mediated depletion of mature cells according to the manufacturer's protocol (StemCell Technologies) using depletion cocktail, including antibodies to CD2, CD3, CD14, CD16, CD19, CD24, CD56, and CD66b. Enriched immature mononuclear cells were double-stained with peridinin chlorophyll protein (PerCP)-conjugated CD34 antibody (Figure 1D) and phycoerythrin (PE)-conjugated CD133 (Figure 1F), CD117 (Figure 1G), or CD135 (Figure 1H) antibody. The number of cells in a region including brightly stained cells was counted, and immature cells were quantified using $CD34^+$ cells as an internal control. The cumulative intra-assay coefficient of variation was 14%, 13%, 14%, and 15%, with $CD34^+$, $CD133^+$, $CD117^+$, and $CD135^+$ cell measurements, respectively, from 5 stroke patients.

Atherosclerosis in the common and internal carotid arteries was analyzed by ultrasonography to determine plaque score as described previously.[7] Cerebral infarcts (diameter >5 mm) were counted independently by a neurologist blinded to other parameters under study (number of circulating $CD34^+$, etc) using T1-weighted, T2-weighted, and fluid-attenuated inversion-recovery MRI obtained with a 1.5-Tesla MRI scanner. The diagnosis of hypoperfusion was made angiographically. Regional cerebral blood flow (CBF), cerebral blood volume, oxygen extraction fraction (OEF), and cerebral metabolic rate of oxygen ($CMRO_2$) were quantified by conventional steady-state ^{15}O PET using a PET scanner (Shimadzu) as described.[8] Cerebrovascular function was evaluated in patients with chronic hypoperfusion caused by major cerebral artery (carotid artery or M1 portion of the middle cerebral artery) occlusion or severe stenoses (>90%) without a major stroke. Twelve patients with 15 major arterial occlusions or stenoses had PET examinations.

To investigate the mobilization of immature cells after acute cerebral infarction, peripheral blood was quantified at 6 hours and 3, 7, 14, and 30 days after the onset of stroke. The episodes of acute cerebral infarction were confirmed by the diffusion image of brain MRI. Age-matched volunteers who had no history of cerebrovascular diseases and no neuronal deficiency were enrolled as controls (mean age, 67±4 years). Test-retest intraclass correlations were 0.88, 0.75, 0.86, and 0.86 for CD34, CD133, CD117, and CD135, respectively, obtained from 5 volunteers tested twice with an interval of at least 10 days between samples.

Univariant correlations were performed using Pearson's correlation coefficient and Spearman's correlation coefficient. Statistical comparisons among groups were determined using analysis of variance. Individual comparisons were performed using Students' *t* test. In all experiments, mean±SE is reported.

Results

First, we investigated mobilization of immature cells after acute cerebral infarction (n=5), focusing on $CD34^+$ cells. The level of $CD34^+$ cells gradually increased to day 7 and remained significantly above the prestroke baseline on days 7 and 14, returning to baseline levels by day 30 (Figure 2A). On the basis of these data, we enrolled 25 patients with a history of atherothrombotic cerebral ischemic events, excluding those who had suffered cerebrovascular or cardiovascular acute ischemic episodes in the 30 days before study, as well as premenopausal females. In this group (>30 days after stroke), no correlation was observed between the interval after stroke and the level of circulating $CD34^+$ cells (r=0.009, P=0.97). Characteristics of this group included mean age of 68±2 years, 20 men and 5 women, 23 patients receiving antiplatelet therapy, 11 patients receiving antihypertensive therapy, 6 patients receiving therapy for hyperlipidemia, 5 patients receiving therapy for diabetes mellitus (DM), and 16 patients with a current or past history of smoking.

Several factors were found to influence the number of circulating $CD34^+$ cells. Statistical analysis revealed a significant decrease in circulating $CD34^+$ cells in patients with DM (0.5±0.1; non-DM, 1.2±0.1 cells/μL; P=0.01). In contrast,

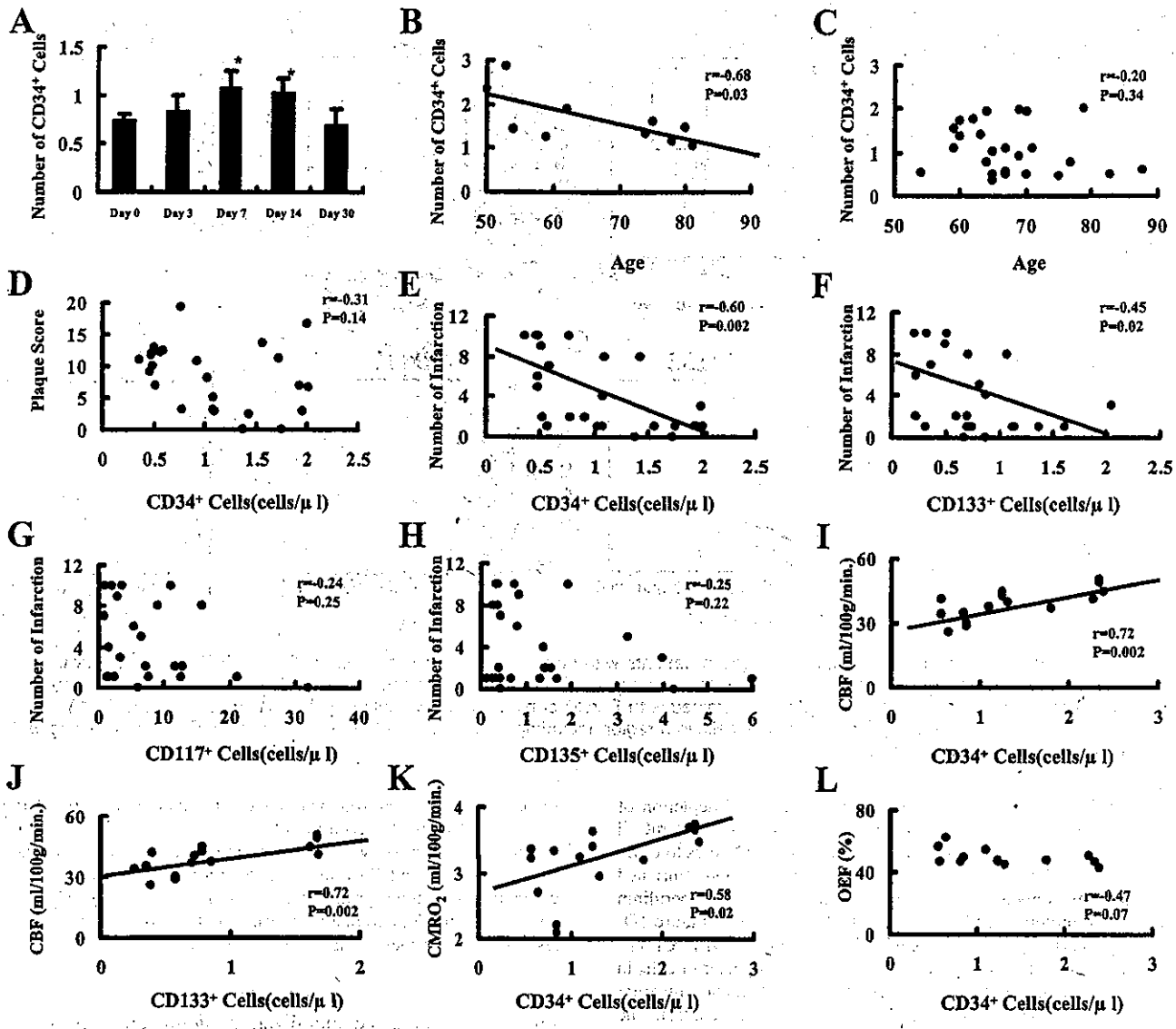

Figure 2. Levels of circulating $CD34^+$ cells and stroke. Circulating $CD34^+$ cells increased after the onset of stroke and peaked on day 7. A significant increase in circulating $CD34^+$ cells was observed on days 7 and 14 (A). A decrease of circulating $CD34^+$ cell was observed with aging in the control group (B), but no such correlation was observed in the stroke patient group (C). No correlation was observed between the number of circulating $CD34^+$ cells and the degree of arteriosclerosis in major cerebral arteries (D). However, there was a correlation between cerebral infarctions and circulating $CD34^+$ (E) and $CD133^+$ cells (F). In contrast, there was no correlation between cerebral infarction and $CD117^+$ (G) or $CD135^+$ cells (H). Correlation between circulating $CD34^+$ (I) and $CD133^+$ (J) cells and CBF in areas of chronic hypoperfusion was observed. Lower levels of circulating $CD34^+$ cells were correlated with a decrease in $CMRO_2$ (K) but not with a change in OEF (L). $^*P<0.05$ compared with day 0 (based on 2-way ANOVA).

no change was observed in patients with hypertension ($P=0.61$), with hyperlipidemia ($P=0.81$), with smoking ($P=0.64$), or based on gender ($P=0.36$). In addition, treatment with HMG-CoA reductase inhibitors ($P=0.81$), compared with patients without hyperlipidemia, did not impact the number of $CD34^+$ cells. In the control patient group, a decrease of circulating $CD34^+$ cells was observed with aging (Figure 2B), although this was not observed in the patient group (Figure 2C). Comparing baseline levels of circulating $CD34^+$ cells, there was a significant decrease in the patient group compared with age-matched controls (stroke, 1.1 ± 0.1; control, 1.6 ± 0.2 cells/μL; $P=0.02$).

We sought a possible correlation between circulating immature cells and the degree of arteriosclerosis of the common and internal carotid arteries in the patients with atherothrombotic cerebral ischemic events. However, there was no significant correlation between arteriosclerosis and circulating $CD34^+$ (Figure 2D). This result was not surprising, because multiple risk factors and cell types contribute to progression of vascular lesions in major arteries. In contrast, because disruption of vascular homeostasis and repair are associated with cerebral infarction, we reasoned that a history of cerebral infarction might correlate with circulating immature cells. A strong correlation was observed between the number of infarcts and the absolute number of circulating $CD34^+$ cells (Figure 2E) and $CD133^+$ cells (Figure 2F). However, no significant correlation with regard to cerebral infarcts was observed with circulating $CD117^+$ cells (Figure 2G) and $CD135^+$ cells (Figure 2H).

In view of the critical role of endothelium in maintaining CBF, we evaluated cerebrovascular function in patients with chronic hypoperfusion. Direct correlations were observed between CBF (in the chronically hypoperfused area) and circulating $CD34^+$ cells (Figure 2I) and $CD133^+$ cells (Figure 2J). In addition, lower numbers of circulating $CD34^+$ cells (Figure 2K) correlated with diminished $CMRO_2$, although there was no significant increase in the OEF (Figure 2L). These observations suggest a contribution of $CD34^+$ cells in homeostasis and repair of the cerebral circulation and maintenance of brain metabolism. No correlation was observed with the above parameters of vascular function and circulating $CD117^+$ and $CD135^+$ cells. Measurement of angiogenic growth factors in patient plasma, vascular endothelial growth factor, basic fibroblast growth factor, hemopoietic growth factor, and insulin-like growth factor-1 also demonstrated no correlation with indices of cerebrovascular function or the number of $CD34^+$ cells (not shown).

Discussion

We have found that circulating immature cell populations, especially $CD34^+$ and $CD133^+$ cells, are associated with maintenance and repair of the cerebral vasculature. In our study, we used a simple and precise method to count the absolute number of circulating $CD34^+$ cells in a small sample of peripheral blood. Our results indicate that the level of $CD34^+$ cells serves as an index/marker for cerebrovascular function. Analysis of $CD133^+$, $CD117^+$, and $CD135^+$ cells, which identify other populations of immature cells, demonstrated that only $CD133^+$ cells correlated with cerebrovascular function in a manner paralleling $CD34^+$ cells.

Patients with diabetes displayed a significant reduction in the number of circulating $CD34^+$ cells. In view of the microvascular dysfunction that is characteristic of diabetes, this may not be surprising. Similarly, decreased circulating $CD34^+$ cells with increasing age in healthy individuals may be associated with limited vascular renewal in older individuals. It was also of interest to note no change between levels of $CD34^+$ cells in patients taking HMG-CoA reductase inhibitors. The latter results might reflect the positive effect of such drugs countering the negative effect of hyperlipidemia on circulating $CD34^+$ cells. Such conclusions, of course, are at best tentative, because in this first report we have identified associations rather than proved a cause-effect relationship.

These observations suggest that diminished numbers of $CD34^+$ and $CD133^+$ cells impact maintenance and repair of cerebral vasculature. Precise measurement of circulating $CD34^+$ cells provides a marker for cerebrovascular function in the setting of ischemic stress.

Acknowledgments

This work was supported by the Uehara, Takeda, Terumo Medical Foundations and KAKENHI (15590785). The sponsors of the study had no role in study design, data collection, data analysis, interpretation, or writing of the report.

References

1. Asahara T, Murohara T, Sullivan A, et al. Isolation of putative progenitor endothelial cells for angiogenesis. *Science*. 1997;275:964–967.
2. Taguchi A, Ohtani M, Soma T, et al. Therapeutic angiogenesis by autologous bone-marrow transplantation in a general hospital setting. *Eur J Vasc Endovasc Surg*. 2003;25:276–278.
3. Tateishi-Yuyama E, Matsubara H, Murohara T, et al. Therapeutic angiogenesis for patients with limb ischaemia by autologous transplantation of bone-marrow cells: a pilot study and a randomised controlled trial. *Lancet*. 2002;360:427–435.
4. Hamano K, Nishida M, Hirata K, et al. Local implantation of autologous bone marrow cells for therapeutic angiogenesis in patients with ischemic heart disease: clinical trial and preliminary results. *Jpn Circ J*. 2001;65:845–847.
5. Majka M, Janowska-Wieczorek A, Ratajczak J, et al. Numerous growth factors, cytokines, and chemokines are secreted by human $CD34^+$ cells, myeloblasts, erythroblasts, and megakaryoblasts and regulate normal hematopoiesis in an autocrine/paracrine manner. *Blood*. 2001;97:3075–3085.
6. Beck H, Voswinckel R, Wagner S, et al. Participation of bone marrow–derived cells in long-term repair processes after experimental stroke. *J Cereb Blood Flow Metab*. 2003;23:709–717.
7. Sasaki T, Watanabe M, Nagai Y, et al. Association of plasma homocysteine concentration with atherosclerotic carotid plaques and lacunar infarction. *Stroke*. 2002;33:1493–1496.
8. Hirano T, Minematsu K, Hasegawa Y, et al. Acetazolamide reactivity on ^{123}I-IMP single photon emission computed tomography in patients with major cerebral artery occlusive disease: correlation with positron emission tomography parameters. *J Cereb Blood Flow Metab*. 1994;14:763–770.

International Congress Series 1270 (2004) 177–180

ELSEVIER

www.ics-elsevier.com

Prolonged interhemispheric neural conduction time evaluated by auditory-evoked magnetic signal and cognitive deterioration in elderly subjects with unstable gait and dizzy sensation

Hiroshi Oe[a,*], Akihiko Kandori[b], Tsuyoshi Miyashita[b], Kuniomi Ogata[b], Naoaki Yamada[c], Keiji Tsukada[d], Kotaro Miyashita[a], Saburo Sakoda[e], Hiroaki Naritomi[a]

[a] *Department of Cerebrovascular Medicine, National Cardiovascular Center, 5-7-1 Fujishiro-dai, Suita, Osaka 565-8565, Japan*
[b] *Central Research Laboratory, Hitachi Ltd., Tokyo, Japan*
[c] *Department of Radiology, National Cardiovascular Center, Osaka, Japan*
[d] *Okayama University, Okayama, Japan*
[e] *Department of Neurology, Osaka University, Osaka, Japan*

Abstract. Magnetoencephalography (MEG) studies have showed that the latency of auditory-evoked neuronal action peak (N100m peak) detected at the temporal cortex ipsilateral to the auditory stimulation is delayed as compared with that detected at the contralateral side. Our recent auditory evoked magnetic fields (AEFs) study has indicated that auditory impulses, originated from the unilateral ear, first arrive at the contralateral temporal cortex and later reach the ipsilateral temporal cortex through interhemispheric neural connections, thus leading to the delay of ipsilateral N100m peak latency. Such a conduction pathway of auditory impulses makes it possible to measure interhemispheric neural conduction time (INCT). We measured INCT in 33 elderly patients (72 ± 10 years of age) complaining of unstable gait and dizzy sensation to study its relationship with cognitive function. Cognitive function was estimated with mini-mental state examination (MMSE) scores. The patients were classified into two groups, such as Group A with normal cognitive function (MMSE score ≥ 24, $n=23$) and Group B with cognitive dysfunction (MMSE score ≤ 23, $n=10$). INCT was significantly longer in Group B (50.5 ± 14.7 ms) than in Group (15.6 ± 13.9 ms, $p<0.05$). In the entire patient group, INCT was prolonged negatively correlating with MMSE scores ($r=-0.84$, $p<0.001$). The results of the present study suggest that the impairment of cognitive function may be closely related with the prolongation of

* Corresponding author. Tel.: +81-6-6833-5012; fax: +81-6-6872-7486.
E-mail address: hirooe@hsp.ncvc.go.jp (H. Oe).

doi:10.1016/j.ics.2004.05.090

INCT. The measurement of INCT with AEFs may be useful for early detection of cognitive impairment in elderly patients with dizziness who may later develop dementia.

Keywords: Auditory evoked magnetic fields; N100m peak latency; Cognitive deterioration; Mini-mental state examination; Dizziness

1. Introduction

Auditory impulses, originating from the unilateral ear, reach the temporal auditory cortex bilaterally [1], although detailed neural pathways are unknown. MEG studies have indicated that the latency of auditory-evoked neuronal action peak (N100m peak) detected at the temporal cortex ipsilateral to the auditory stimulation is always delayed as compared with that detected at the contralateral side [2]. Regarding this phenomenon, our recent MEG study has suggested that auditory impulses originating from the unilateral ear first arrive at the contralateral temporal cortex and later reach the ipsilateral temporal cortex through interhemispheric neural connections, thus leading to the delay of ipsilateral N100m peak latency [3]. Such a conduction manner of auditory impulses enables us to measure interhemispheric neural conduction time (INCT) with MEG. We estimated the INCT, using MEG, in elderly patients with unstable gait and dizziness and studied its relationship with cognitive function.

2. Subjects and methods

2.1. Subjects

Thirty-three patients (18 males and 15 females, 72 ± 10 years of age) complaining of unstable gait and dizzy sensation, who had otherwise no focal neurological abnormality, were subjected. We excluded patients with auditory impairments at 30 dB or less in 1000 Hz pure tone audiograms or abnormal findings in otorhinologic examinations, caloric test and auditory brain stem response.

2.2. Methods

MEG studies were performed using a superconducting quantum interference device (SQUID) system (MC-6400, Hitachi) with 64 co-axial gradiometer (8×8 matrix) in a two-dimensional plane. Auditory stimuli with 90 dB normal hearing level in intensity and 1 kHz tone burst were provided in the right ear, and N100m peak latency was measured at both temporal cortices (Fig. 1). Cognitive function was estimated by measurement of the mini-mental state examination (MMSE) score. The patients were classified into two groups, according to MMSE scores as follows: Group A with normal cognitive function (MMSE scores $\geqslant 24$) and Group B with cognitive dysfunction (MMSE scores $\leqslant 23$). The INCT (ms) was calculated from the